



# Spectroscopic Determination of Stellar Parameters and Oxygen Abundances for Hyades/Field G–K Dwarfs

Yoichi Takeda<sup>1,2</sup> and Satoshi Honda<sup>3</sup><sup>1</sup> National Astronomical Observatory, 2-21-1 Osawa, Mitaka, Tokyo 181-8588, Japan; [takeda.yoichi@nao.ac.jp](mailto:takeda.yoichi@nao.ac.jp), [takedayoichi.vega@gmail.com](mailto:takedayoichi.vega@gmail.com)<sup>2</sup> SOKENDAI, The Graduate University for Advanced Studies, 2-21-1 Osawa, Mitaka, Tokyo 181-8588, Japan<sup>3</sup> Nishi-Harima Astronomical Observatory, Center for Astronomy, University of Hyogo, 407-2 Nishigaichi, Sayo-cho, Sayo, Hyogo 679-5313, Japan; [honda@nhao.jp](mailto:honda@nhao.jp)

Received 2019 December 18; revised 2020 February 19; accepted 2020 February 21; published 2020 March 30

## Abstract

It has been suggested that Fe abundances of K dwarfs derived from Fe I and Fe II lines show considerable discrepancies, and oxygen abundances determined from high-excitation O I 7771–5 triplet lines are appreciably overestimated (the problem becoming more serious toward lower  $T_{\text{eff}}$ ), which, however, has not yet been widely confirmed. With the aim of clarifying this issue, we spectroscopically determined the atmospheric parameters of 148 G–K dwarfs (Hyades cluster stars and field stars) by assuming the classical Fe I/Fe II ionization equilibrium as usual, and determined their oxygen abundances by applying the non-local thermal equilibrium spectrum fitting analysis to O I 7771–5 lines. It turned out that the resulting parameters did not show any significant inconsistency with those determined by other methods (for example, the mean differences in  $T_{\text{eff}}$  and  $\log g$  from the well-determined solutions of Hyades dwarfs are mostly  $\lesssim 100$  K and  $\lesssim 0.1$  dex). Likewise, the oxygen abundances of Hyades stars are around  $[\text{O}/\text{H}] \sim +0.2$  dex (consistent with the metallicity of this cluster) without exhibiting any systematic  $T_{\text{eff}}$ -dependence. Accordingly, we conclude that parameters can be spectroscopically evaluated to a sufficient precision in the conventional manner (based on the Saha–Boltzmann equation for Fe I/Fe II) and oxygen abundances can be reliably determined from the O I 7771–5 triplet for K dwarfs as far as stars of  $T_{\text{eff}} \gtrsim 4500$  K are concerned. We suspect that previously reported strongly  $T_{\text{eff}}$ -dependent discrepancies may have stemmed mainly from overestimation of weak-line strengths and/or improper  $T_{\text{eff}}$  scale.

*Unified Astronomy Thesaurus concepts:* [Stellar abundances \(1577\)](#); [Stellar atmospheres \(1584\)](#); [Fundamental parameters of stars \(555\)](#); [Late-type stars \(909\)](#); [Open star clusters \(1160\)](#)

*Supporting material:* [tar.gz file](#)

## 1. Introduction

It has been reported by several investigators that significant difficulties are involved in the spectroscopic analysis of lower main-sequence stars of late G to K type (hereinafter we refer to this star group simply as “K dwarfs”). That is, the Fe abundances derived from lines of neutral and ionized stages (Fe I and Fe II) are not consistent with each other (generally the latter are larger than the former), and this Fe II versus Fe I discrepancy becomes progressively more serious as the effective temperature ( $T_{\text{eff}}$ ) is lowered. See, e.g., Allende Prieto et al. (2004; their Figure 8), Kotoneva et al. (2006; their Figure 9), and Luck (2017, his 1) for field stars; King & Schuler (2005; their Figure 4) for UMa moving group stars; Yong et al. (2004; their Figure 4) and Schuler et al. (2006a; their Figure 3) for Hyades cluster stars; Schuler et al. (2010; their Figure 1) for Pleiades cluster stars. Whichever reason is relevant for this trend (e.g., substantial non-local thermal equilibrium (non-LTE) overionization effect related to stellar activity; see Takeda 2008), it must have a large impact if it is real, given the paramount importance of Fe lines in stellar spectroscopy. For example, the widely used method of determining the atmospheric parameters of solar-type stars based on Fe I and Fe II lines (which makes use of the excitation equilibrium of Fe I and ionization equilibrium of Fe I/Fe II; e.g., Takeda et al. 2002) would hardly be applicable to K dwarfs, since classical 1D plane-parallel model atmospheres would be no longer valid for them.

However, some doubt remains regarding whether this effect is really so important. Wang et al. (2009) carried out

spectroscopic analysis of 30 nearby lower main-sequence stars at  $4700 \lesssim T_{\text{eff}} \lesssim 5400$  K. They could not confirm the appreciable  $T_{\text{eff}}$ -dependent systematic discrepancy reported by Kotoneva et al. (2006), but found a reasonable consistency between Fe I and Fe II abundances to a level of  $\lesssim 0.1$  dex (see their Figure 5). Furthermore, Aleo et al. (2017) conducted an extensive examination on this alleged “Fe abundance anomaly in K dwarfs” by carefully determining the Fe abundances from lines of neutral and ionized stages for 63 wide binary stars and 33 Hyades stars at  $4300 \lesssim T_{\text{eff}} \lesssim 6100$  K. Their important finding is the importance of the line-blending effect for certain Fe II lines, which becomes prominent for K dwarfs of lower  $T_{\text{eff}}$  where Fe II lines are weaker while lines of neutral metals get stronger. By removing these lines, they found that the Fe II–Fe I discrepancy is appreciably mitigated; e.g., for Hyades stars, only  $\sim 0.1$  dex at  $4500 \text{ K} \lesssim T_{\text{eff}}$ , though this increases to  $\sim 0.3$  dex at further lower  $T_{\text{eff}}$  of  $\sim 4300$  K (see their Figure 9). Likewise, Tsantaki et al. (2019) very recently performed a detailed study on the Fe ionization equilibrium based on the spectra of 451 FGK-type stars (subsample of the HARPS GTO planet survey program) and also arrived at the conclusion that unresolved line blending is probably the main reason for the apparent overabundance of Fe II. They showed that consistent  $T_{\text{eff}}$ -independent results could be obtained by rejecting suspicious Fe II lines. These two recent investigations suggest that the considerably large Fe II–Fe I disagreement reported in previous studies (e.g., as much as  $\sim 0.5$ – $0.6$  dex at  $T_{\text{eff}} \sim 4500$  K for the case of Hyades K dwarfs; see Yong et al. 2004; Schuler et al. 2006a) is likely to be due to their

inadequate choice of blending-affected Fe II lines, leading to a significant overestimation of Fe II abundances.

This revelation reminded us of a similar problem related to oxygen abundance determination for K dwarfs. That is, the widely used high-excitation O I 7771–5 triplet lines tend to result in erroneously overestimated abundances (being progressively more serious with a decrease in  $T_{\text{eff}}$ ), which was reported in several studies on open cluster stars: UMa moving group (King & Schuler 2005; their Figure 4), M34 as well as Pleiades (Schuler et al. 2004; their Figures 1 and 2), Hyades (Schuler et al. 2006b; their Figure 3), and NGC 752 (Maderak et al. 2013; their Figure 5). Actually, this effect of abundance anomaly they found was surprisingly large, because [O/H] values (oxygen abundance relative to the Sun) of K dwarfs derived from O I 7771–5 lines turned out to be unreasonably higher than those of G dwarfs by as much as  $\lesssim 1$  dex, despite the fact that they should have similar values for stars belonging to the same cluster.

Although their investigations were based on the assumption of LTE, the non-LTE effect evaluated in the standard manner using classical model atmospheres (see, e.g., Takeda 2003) cannot explain this apparently large overabundance of [O/H], because non-LTE correction is strength-dependent and almost negligible for K dwarfs, where high-excitation O I 7771–5 lines are considerably weak because of lower  $T_{\text{eff}}$ . So, if this is real, it might be due to some kind of non-classical activity-related phenomenon such as the intensification caused by chromospheric temperature rise (see Takeda 2008). However, in view of the similarity to the case of Fe abundance discrepancy (in the sense that considerably weak Fe II and O I lines are involved in the anomalous abundances seen in K dwarfs), this problem on the reliability of O I 7771–5 triplet may be worth reinvestigation.

This situation motivated us to revisit these “spectroscopic K dwarf problems on Fe and O abundances” based on the spectral data for a large sample of G–K dwarfs (47 Hyades stars and 101 field stars). Our approach is simply to apply the standard method of analysis adopted in our previous studies to all these sample stars and see if any unreasonable result (such as suggesting the breakdown of classical modeling) emerges or not. More precisely, what we attempt to do and clarify in this investigation is as follows.

1. We determine the atmospheric parameters of each program star in the conventional manner from the equivalent widths of Fe I and Fe II lines while assuming LTE (Saha–Boltzmann equation) as done by Takeda et al. (2005). If the classical treatment is not valid for K dwarfs, the resulting parameters would reveal some kind of  $T_{\text{eff}}$ -dependent inconsistency between G and K dwarfs. In this context, Hyades stars should play an especially important role, because their parameters are known to sufficient precision. Comparison of our spectroscopically determined parameters and those already established by other methods would provide a decisive touchstone.<sup>4</sup>
2. By using the model atmospheres corresponding to such determined atmospheric parameters, we then evaluate the

oxygen abundance for each star by applying the spectrum-fitting method to O I 7771–5 (see, e.g., Takeda et al. 2015), where the non-LTE effect is taken into account according to Takeda’s (2003) calculation. Again, Hyades stars can serve as a good testbed, because they are considered to have practically the same O abundances. Are the resulting [O/H] values consistent with each other? Or do they show such considerable  $T_{\text{eff}}$ -dependent disagreement as concluded by Schuler et al. (2006b)? This must be an interesting check. In addition, it is worthwhile to examine the behavior of [O/Fe] ( $\equiv$ [O/H]–[Fe/H]) ratios with a change in [Fe/H] (metallicity) obtained for field stars. Is the [O/Fe] versus [Fe/H] diagram obtained from O I 7771–5 lines for K dwarfs consistent with that derived by Takeda & Honda (2005) for F–G stars with the same triplet? This can be another touchstone for judging the reliability of these high-excitation O I lines in the context of oxygen abundance determination for K dwarfs.

## 2. Observational Data

As the target stars of this investigation, we adopted a sample of 148 dwarfs (consisting of 47 Hyades cluster stars and 101 field stars), which are in the apparent magnitude range of  $V \sim 5\text{--}10$ . Regarding the Hyades stars, since we intended to cover a rather wider range of spectral type (in order to clarify the  $T_{\text{eff}}$ -dependence), main-sequence stars in the color range  $0.5 \lesssim B - V \lesssim 1.2$  (corresponding to late F through mid K) were selected from the list of de Bruijne et al. (2001). As to field stars, we mainly invoked the Kotoneva et al. (2002) list of G–K dwarfs, from which 99 stars in the color range  $0.7 \lesssim B - V \lesssim 1.2$  (corresponding to mid-late G through mid K) were chosen. In addition, in order to reinforce the sample of mid-K stars, 61 Cyg A and  $\xi$  Boo B (both having  $B - V \sim 1.2$ ) were also included. The basic data of these 148 stars are summarized in Table 1 (and in “tableE1.dat” in the supplementary .tar.gz package). The  $M_V$  versus  $B - V$  diagram for the program stars is shown in Figure 1(a).

Our spectroscopic observations for 118 stars were done in four runs over 2010–2011 (2010 April/May, 2010 August, 2010 November/December, and 2011 November) using the HIDES (HIgh Dispersion Echelle Spectrograph) placed at the coude focus of the 188 cm reflector at Okayama Astrophysical Observatory. Equipped with three mosaicked  $4\text{K} \times 2\text{K}$  CCD detectors at the camera focus, HIDES enabled us to obtain an echellogram covering  $\sim 5100\text{--}8800 \text{ \AA}$  with a resolving power of  $R \sim 67,000$ . The observations for the remaining 30 stars were done on 2014 September 9 with the High Dispersion Spectrograph at the Nasmyth platform of the 8.2 m Subaru Telescope, by which high-dispersion spectra with a resolution of  $R \simeq 80,000$  covering  $\sim 5100\text{--}7800 \text{ \AA}$  (with two  $4\text{K} \times 2\text{K}$  CCDs) were obtained. The observed dates for each of the program stars are given in “tableE1.dat.”

The reduction of the spectra (bias subtraction, flat-fielding, scattered-light subtraction, spectrum extraction, wavelength calibration, and continuum normalization) was performed using the “echelle” package of the software IRAF<sup>5</sup> in the standard

<sup>4</sup> Although Takeda (2008) once conducted this reliability test of spectroscopic parameters using Hyades stars of  $5100 \text{ K} \lesssim T_{\text{eff}} \lesssim 6200 \text{ K}$ , few K-type dwarfs of main interest to us were included, unfortunately. Besides, the spectra used at that time (later analyzed also by Takeda et al. 2013) were limited to the wavelength range of  $\sim 6000\text{--}7200 \text{ \AA}$  and thus not necessarily sufficient in view of the number of available Fe I and Fe II lines. Therefore, we decided to redo this task using new observational data with wider wavelength coverage.

<sup>5</sup> IRAF is distributed by the National Optical Astronomy Observatories, which is operated by the Association of Universities for Research in Astronomy, Inc. under cooperative agreement with the National Science Foundation.

**Table 1**  
Basic Data, Parameters, and Abundance Results of 148 Program Stars

HIP (1)	HD (2)	$V$ (3)	$M_V$ (4)	$B - V$ (5)	$T_{\text{eff}}$ (6)	$\log g$ (7)	$v_t$ (8)	[Fe/H] (9)	$v_M$ (10)	[O/H] (11)	$\Delta_{7774}$ (12)	$W_{7774}$ (13)
Hyades stars												
19796	26784	7.11	3.73	0.51	6307	4.29	1.37	0.26	13.74	0.19	-0.23	125.4
22566	30809	7.90	4.07	0.53	6250	4.29	1.10	0.24	9.06	0.14	-0.21	113.1
19386	26257	7.64	3.57	0.55	6201	4.26	1.03	0.23	6.31	0.12	-0.21	108.2
20557	27808	7.13	4.07	0.52	6199	4.27	1.21	0.19	10.45	0.17	-0.21	114.9
20815	28205	7.41	4.11	0.54	6180	4.35	1.07	0.19	8.67	0.22	-0.20	113.2
25639	35768	8.50	3.82	0.56	6138	4.08	1.13	0.15	5.83	0.06	-0.23	105.8
20237	27406	7.46	4.20	0.56	6134	4.37	1.07	0.27	9.59	0.19	-0.18	106.8
15304	20430	7.38	3.91	0.57	6125	4.29	0.99	0.33	5.97	0.17	-0.18	104.5
10672	14127	8.55	4.48	0.57	6125	4.41	0.88	0.01	6.58	-0.05	-0.16	84.2
22422	30589	7.72	4.19	0.58	6081	4.39	0.97	0.24	5.54	0.07	-0.15	90.9
19148	25825	7.85	4.50	0.59	6078	4.47	1.05	0.21	6.14	0.06	-0.14	87.8
15310	20439	7.78	4.46	0.62	6003	4.48	1.01	0.31	5.99	0.16	-0.14	89.3
20577	27859	7.79	4.37	0.60	5955	4.30	0.96	0.14	6.44	0.11	-0.16	87.5
21317	28992	7.90	4.73	0.63	5928	4.48	0.98	0.20	5.55	0.13	-0.12	81.5
19786	26767	8.05	4.78	0.64	5922	4.42	1.07	0.23	5.60	0.08	-0.12	79.4
20899	28344	7.83	4.45	0.61	5902	4.30	1.11	0.15	6.68	0.15	-0.15	86.9
20741	28099	8.10	4.75	0.66	5852	4.55	0.92	0.24	4.42	0.12	-0.10	72.6
19793	26736	8.05	4.73	0.66	5815	4.38	0.99	0.22	5.78	0.12	-0.12	74.6
19781	26756	8.45	5.15	0.69	5745	4.54	0.91	0.22	5.13	0.08	-0.09	62.7
20146	27282	8.47	5.11	0.72	5677	4.48	0.93	0.24	5.32	0.09	-0.09	60.0
23750	240648	8.82	5.19	0.73	5630	4.57	0.89	0.25	5.38	0.12	-0.07	56.5
14976	19902	8.15	5.03	0.73	5614	4.57	0.91	0.18	3.72	0.08	-0.07	53.7
20130	27250	8.62	5.48	0.74	5591	4.55	1.00	0.18	4.59	0.08	-0.07	52.6
23069	31609	8.89	5.36	0.74	5583	4.53	0.84	0.21	3.87	0.10	-0.07	53.1
24923	242780	9.03	5.34	0.77	5560	4.57	0.85	0.27	5.04	0.12	-0.07	52.0
21099	28593	8.59	5.28	0.73	5557	4.44	0.99	0.17	4.68	0.07	-0.08	52.2
23498	32347	9.00	5.33	0.77	5549	4.52	1.03	0.21	4.96	0.05	-0.07	49.2
20949	283704	9.19	5.35	0.77	5544	4.57	0.88	0.23	3.75	0.09	-0.07	49.3
20480	27732	8.84	5.41	0.76	5539	4.49	1.00	0.15	4.55	0.11	-0.07	52.2
21741	284574	9.40	5.42	0.81	5425	4.55	0.95	0.23	5.00	0.17	-0.06	46.2
19934	284253	9.14	5.59	0.81	5376	4.57	0.87	0.17	3.71	0.15	-0.05	41.9
20951	285773	8.95	5.87	0.83	5350	4.57	1.02	0.14	3.90	0.12	-0.05	39.6
22380	30505	8.98	5.63	0.83	5336	4.57	0.94	0.21	4.49	0.19	-0.05	41.1
20850	28258	9.02	5.66	0.84	5321	4.50	1.04	0.18	4.19	0.15	-0.05	39.9
20492	27771	9.11	5.74	0.85	5292	4.60	0.89	0.22	4.38	0.01	-0.04	31.2
20978	28462	9.08	6.04	0.86	5242	4.50	1.04	0.16	4.74	0.09	-0.04	33.3
18327	285252	8.99	5.91	0.90	5183	4.61	1.02	0.21	4.27	0.18	-0.04	31.9
19098	285367	9.31	5.79	0.89	5123	4.56	1.03	0.11	4.41	0.24	-0.04	31.6
23312	...	9.71	5.83	0.96	5104	4.53	0.90	0.14	4.00	0.22	-0.04	30.1
20827	285830	9.48	5.67	0.93	5089	4.61	0.89	0.23	3.88	0.22	-0.03	28.2
20082	285690	9.57	6.08	0.98	5030	4.53	0.79	0.15	3.60	0.01	-0.03	21.7
19263	285482	9.94	6.41	1.00	4898	4.50	0.85	0.07	4.24	0.03	-0.02	17.0
22654	284930	10.29	6.68	1.07	4831	4.47	0.99	0.11	4.22	-0.07	-0.02	12.5
18946	...	10.12	6.94	1.09	4823	4.64	0.92	0.16	3.46	-0.05	-0.01	11.5
20762	286789	10.48	7.18	1.15	4729	4.25	1.15	-0.02	4.51	-0.20	-0.02	9.0
18322	286363	10.12	7.24	1.07	4725	4.71	0.91	0.17	3.97	0.31	-0.01	14.2
19441	...	10.10	7.47	1.19	4525	4.61	0.70	0.14	3.56	0.11	-0.01	6.3
Field stars												
053471	94718	8.45	5.58	0.73	5482	4.45	0.73	-0.03	3.47	-0.13	-0.06	37.2
082588	152391	6.65	5.51	0.75	5475	4.50	0.94	0.02	4.15	-0.01	-0.06	42.0
004907	5996	7.67	5.61	0.76	5445	4.53	0.96	-0.09	3.68	-0.05	-0.06	38.6
010818	14374	8.48	5.51	0.74	5444	4.58	0.80	-0.01	3.42	-0.02	-0.05	38.4
026653	37216	7.85	5.63	0.76	5441	4.58	0.94	-0.03	3.48	-0.02	-0.05	38.5
059280	105631	7.46	5.53	0.79	5439	4.50	0.88	0.19	3.57	0.01	-0.06	40.5
040419	69076	8.27	5.61	0.71	5434	4.47	0.66	-0.24	3.47	-0.23	-0.05	31.3
093926	178450	7.78	5.54	0.76	5423	4.45	2.00	-0.04	18.51	0.24	-0.07	57.4
043852	76218	7.69	5.60	0.77	5422	4.59	0.83	0.03	4.34	-0.04	-0.05	35.9
094346	180161	7.04	5.53	0.80	5418	4.49	0.95	0.17	3.67	0.11	-0.06	44.2
055210	98281	7.29	5.58	0.73	5401	4.47	0.75	-0.21	3.24	-0.15	-0.05	33.1
112245	215500	7.50	5.50	0.72	5399	4.39	0.62	-0.20	3.15	-0.15	-0.06	33.8
046843	82443	7.05	5.80	0.78	5393	4.65	1.27	-0.03	5.38	0.07	-0.05	39.5
098677	190067	7.15	5.72	0.71	5376	4.48	0.64	-0.32	3.23	-0.37	-0.04	24.4

**Table 1**  
(Continued)

HIP (1)	HD (2)	$V$ (3)	$M_V$ (4)	$B - V$ (5)	$T_{\text{eff}}$ (6)	$\log g$ (7)	$v_t$ (8)	[Fe/H] (9)	$v_M$ (10)	[O/H] (11)	$\Delta_{7774}$ (12)	$W_{7774}$ (13)
065515	116956	7.29	5.59	0.80	5372	4.51	1.07	0.14	5.30	0.11	-0.05	41.5
115331	220182	7.36	5.66	0.80	5368	4.56	1.08	0.06	4.98	0.01	-0.05	36.3
007576	10008	7.66	5.79	0.80	5358	4.52	0.97	-0.03	3.48	-0.11	-0.04	31.6
062016	110514	8.04	5.61	0.80	5358	4.49	0.73	-0.01	3.40	-0.01	-0.05	35.4
075277	136923	7.16	5.64	0.80	5357	4.56	0.67	-0.05	3.35	-0.06	-0.04	32.4
010798	14412	6.33	5.81	0.72	5357	4.51	0.73	-0.49	3.30	-0.35	-0.04	24.9
010276	13483	8.46	5.81	0.78	5347	4.54	0.85	-0.17	3.41	-0.08	-0.05	31.9
042074	72760	7.32	5.63	0.79	5344	4.59	0.92	0.09	3.64	0.07	-0.04	36.4
050782	89813	7.78	5.64	0.75	5336	4.51	0.67	-0.07	3.28	-0.11	-0.04	30.3
081813	151541	7.56	5.63	0.77	5334	4.42	0.66	-0.14	3.40	-0.17	-0.05	29.6
028954	41593	6.76	5.81	0.81	5332	4.50	1.04	0.05	4.54	0.00	-0.05	34.7
106122	204814	7.93	5.56	0.76	5327	4.44	0.66	-0.20	3.18	0.09	-0.06	39.4
000400	225261	7.82	5.78	0.76	5323	4.49	0.62	-0.38	3.25	-0.12	-0.05	30.3
077408	141272	7.44	5.79	0.80	5304	4.45	1.01	0.02	4.20	-0.07	-0.05	31.3
051819	90343	7.29	5.68	0.82	5303	4.50	0.78	0.12	3.50	0.04	-0.05	34.2
014023	18702	8.11	5.56	0.84	5280	4.47	0.74	0.18	3.09	0.21	-0.05	40.0
085235	158633	6.44	5.90	0.76	5270	4.54	0.60	-0.41	3.05	-0.26	-0.04	24.5
074702	135599	6.92	5.96	0.83	5250	4.63	0.90	-0.04	4.05	-0.01	-0.04	28.6
116085	221354	6.76	5.63	0.84	5246	4.53	0.64	0.10	3.01	0.17	-0.04	35.6
072200	130215	7.98	5.87	0.87	5244	4.56	0.88	0.13	3.42	0.05	-0.04	31.0
039157	65583	6.97	5.84	0.72	5243	4.54	0.53	-0.71	3.00	-0.11	-0.05	27.3
082267	151877	8.40	5.85	0.82	5237	4.59	0.69	-0.10	3.04	-0.09	-0.04	25.9
002742	3141	8.02	5.71	0.87	5225	4.51	0.69	0.18	3.04	0.13	-0.04	32.9
012926	17190	7.89	5.84	0.84	5224	4.61	0.61	-0.05	3.10	-0.03	-0.04	26.8
033848	52456	8.16	5.90	0.86	5212	4.51	0.69	0.06	3.25	-0.02	-0.04	27.6
078241	143291	8.02	5.94	0.76	5208	4.40	0.50	-0.40	3.22	-0.20	-0.04	24.0
039064	65430	7.68	5.86	0.83	5202	4.55	0.57	-0.09	2.99	0.09	-0.04	30.5
008543	11130	8.06	5.92	0.76	5197	4.52	0.52	-0.57	2.92	-0.13	-0.04	24.7
000184	224983	8.48	5.85	0.89	5195	4.55	0.73	0.13	2.94	0.02	-0.04	27.5
061099	108984	7.91	5.90	0.86	5194	4.54	0.60	0.11	3.14	0.09	-0.04	29.6
010532	13977	9.11	5.79	0.88	5188	4.58	0.72	0.11	3.20	0.06	-0.04	28.2
066781	119332	7.77	5.89	0.83	5187	4.46	0.68	-0.03	3.21	0.00	-0.04	27.9
054906	97658	7.76	6.12	0.84	5175	4.58	0.61	-0.27	3.05	-0.25	-0.03	20.4
006379	7924	7.17	6.04	0.83	5173	4.60	0.65	-0.15	2.99	-0.07	-0.03	25.8
007830	10261	8.92	5.84	0.91	5165	4.59	0.88	0.04	3.50	0.01	-0.03	27.1
015099	20165	7.83	6.09	0.86	5164	4.56	0.65	0.01	3.11	0.01	-0.03	25.9
073005	132142	7.77	5.88	0.79	5157	4.53	0.38	-0.38	2.98	0.00	-0.04	26.6
013891	18450	8.21	5.93	0.87	5154	4.55	0.56	-0.06	3.02	0.03	-0.04	26.4
006613	8553	8.49	5.89	0.91	5129	4.61	0.59	0.00	2.99	-0.02	-0.03	24.7
112527	216520	7.53	6.03	0.87	5123	4.52	0.57	-0.14	3.12	-0.19	-0.03	20.8
064457	114783	7.56	6.01	0.93	5121	4.47	0.69	0.13	3.03	0.06	-0.04	26.5
036704	59747	7.68	6.21	0.86	5120	4.60	0.85	0.03	3.36	0.10	-0.03	28.0
114886	219538	8.07	6.15	0.87	5110	4.56	0.65	0.01	2.98	-0.02	-0.03	24.4
090790	170657	6.81	6.21	0.86	5087	4.38	0.64	-0.17	3.45	-0.14	-0.04	22.2
012158	16287	8.10	6.17	0.94	5081	4.54	1.00	0.14	3.91	0.03	-0.03	24.0
072312	130307	7.76	6.29	0.89	5078	4.55	0.75	-0.15	3.44	-0.18	-0.03	18.6
098505	189733	7.67	6.25	0.93	5076	4.42	1.06	0.03	4.14	-0.06	-0.03	22.5
053486	94765	7.37	6.15	0.92	5076	4.59	0.94	0.06	3.82	0.05	-0.03	24.0
013976	18632	7.97	6.12	0.93	5075	4.59	0.98	0.19	3.85	0.17	-0.03	27.5
098828	190470	7.82	6.15	0.92	5071	4.62	0.77	0.17	3.04	0.14	-0.03	26.6
026505	37008	7.74	6.18	0.83	5054	4.58	0.09	-0.41	2.79	-0.02	0.01	22.8
108156	208313	7.73	6.19	0.91	5051	4.59	0.72	-0.01	3.04	0.02	-0.03	22.5
108028	208038	8.18	6.28	0.94	5035	4.62	0.84	-0.05	3.57	0.01	-0.03	21.2
011083	14687	8.83	6.18	0.91	5033	4.58	0.59	0.08	2.94	0.04	-0.03	22.4
057939	103095	6.42	6.61	0.75	5033	4.38	-0.10	-1.27	3.28	-0.93	-0.03	5.1
017420	23356	7.10	6.36	0.93	5030	4.57	0.80	-0.08	3.11	-0.14	-0.03	17.6
088972	166620	6.38	6.15	0.88	5019	4.62	0.28	-0.15	2.73	0.05	-0.03	22.4
098792	190404	7.28	6.32	0.81	5016	4.65	-0.18	-0.57	2.93	-0.16	-0.03	16.6
003206	3765	7.36	6.17	0.94	5000	4.53	0.77	0.14	3.02	0.15	-0.03	24.4
092919	175742	8.16	6.50	0.91	4983	4.48	2.13	-0.10	11.88	0.34	-0.04	31.6
049699	87883	7.56	6.28	0.96	4980	4.62	0.56	0.11	2.79	0.11	-0.03	21.7
071395	128311	7.48	6.38	0.97	4967	4.67	0.88	0.16	4.03	0.15	-0.02	20.9
003535	4256	8.03	6.32	0.98	4954	4.47	0.75	0.26	3.06	0.15	-0.03	22.7

**Table 1**  
(Continued)

HIP (1)	HD (2)	$V$ (3)	$M_V$ (4)	$B - V$ (5)	$T_{\text{eff}}$ (6)	$\log g$ (7)	$v_t$ (8)	[Fe/H] (9)	$v_M$ (10)	[O/H] (11)	$\Delta_{7774}$ (12)	$W_{7774}$ (13)
084195	155712	7.95	6.39	0.94	4947	4.43	0.57	-0.10	3.16	-0.07	-0.03	17.9
072146	130004	7.87	6.42	0.93	4930	4.57	0.49	-0.24	2.97	-0.17	-0.02	13.9
033852	51866	7.98	6.43	0.99	4927	4.56	0.69	0.10	3.15	0.01	-0.02	17.2
084616	156985	7.93	6.59	1.02	4916	4.39	0.61	-0.06	3.31	-0.30	-0.02	12.0
035872	57901	8.19	6.20	0.96	4908	4.58	0.53	0.17	2.91	0.25	-0.03	22.4
068184	122064	6.49	6.47	1.04	4908	4.49	0.67	0.23	3.13	0.09	-0.02	19.0
066147	117936	7.98	6.65	1.03	4872	4.28	0.95	0.01	3.63	-0.18	-0.02	13.3
071181	128165	7.24	6.60	1.00	4868	4.60	0.78	-0.03	2.97	-0.08	-0.02	12.8
046580	82106	7.20	6.68	1.00	4861	4.59	0.88	-0.02	3.55	0.12	-0.02	16.7
000974	...	8.73	6.68	1.04	4852	4.67	0.57	0.02	3.00	0.02	-0.02	13.8
023311	32147	6.22	6.49	1.05	4815	4.49	0.66	0.29	2.95	0.28	-0.02	19.4
069526	124642	8.03	6.84	1.06	4798	4.51	0.90	0.10	4.00	0.03	-0.02	13.2
010416	13789	8.55	6.75	1.05	4782	4.64	0.86	0.09	3.31	0.02	-0.01	11.6
105038	202575	7.88	6.84	1.02	4777	4.66	0.75	-0.07	3.57	0.04	-0.01	11.9
032010	47752	8.08	6.86	1.02	4776	4.53	0.78	-0.17	3.16	-0.06	-0.02	11.2
025220	35171	7.93	7.15	1.10	4757	4.43	1.06	-0.10	4.04	-0.20	-0.02	8.9
008275	10853	8.91	7.10	1.04	4739	4.73	0.66	-0.10	3.29	0.00	-0.01	9.8
011000	14635	9.07	6.93	1.08	4732	4.71	0.70	0.19	3.40	0.17	-0.01	12.1
015919	21197	7.86	6.96	1.15	4717	4.22	0.89	0.14	3.34	0.07	-0.02	13.3
005286	6660	8.41	6.83	1.12	4716	4.45	0.72	0.20	3.25	0.01	-0.01	10.7
098698	190007	7.46	6.87	1.13	4677	4.50	0.79	0.22	3.34	0.10	-0.01	10.5
013258	17660	8.87	7.12	1.19	4643	4.32	0.67	0.23	3.25	0.27	-0.02	13.5
104214	201091	5.21	7.49	1.18	4523	4.57	0.32	-0.28	3.18	-0.15	-0.01	4.4
...	131156B	6.82	7.67	1.17	4495	4.55	0.67	-0.25	3.59	-0.12	-0.01	4.2

**Note.** (1) Hipparcos Catalog number. (2) Henry-Draper Catalog number. (3) Apparent visual magnitude (in mag). (4) Absolute visual magnitude (in mag). (5)  $B - V$  color (in mag). (6) Effective temperature (in K). (7) Logarithmic surface gravity ( $\text{cm s}^{-2} \text{dex}^{-1}$ ). (8) Microturbulent velocity dispersion (in  $\text{km s}^{-1}$ ). (9) Fe abundance relative to the Sun (in dex). (10) Macrobroadening velocity (in  $\text{km s}^{-1}$ ). (11) Non-LTE oxygen abundance relative to the Sun,  $A^{\text{NLTE}}(\text{O}) - 8.861$  (in dex), where 8.861 is the solar non-LTE oxygen abundance derived in the same manner (see Takeda et al. 2015). (12) Non-LTE correction ( $\equiv A^{\text{N}} - A^{\text{L}}$ ) (in dex) for O I 7774.166 (middle line of the triplet). (13) Equivalent width for O I 7774.166 (in mÅ). In each stellar group (47 Hyades stars and 101 field stars), the data are arranged in decreasing order of  $T_{\text{eff}}$  similarly to Figures 4 and 5, so that a direct comparison may be possible. (See “tableE1.dat” of the supplementary .tar.gz package for the data arranged in the increasing order of HIP number for each group).

manner. If a few consecutive exposures were done for a star in a night, we co-added these to improve the signal-to-noise ratio (S/N). The average S/N of the finally resulting spectrum is typically  $\sim 100$ – $300$  for most cases.

### 3. Stellar Parameters

#### 3.1. Atmospheric Parameters Based on Fe Lines

The four parameters ( $T_{\text{eff}}$  (effective temperature),  $\log g$  (logarithmic surface gravity),  $v_t$  (microturbulent velocity dispersion), and [Fe/H] (Fe abundance relative to the Sun)) were spectroscopically determined from the equivalent widths ( $W_\lambda$ ) of Fe I and Fe II lines based on the principle and algorithm described in Takeda et al. (2002), which requires that (i) Fe I abundances do not depend upon  $\chi_{\text{low}}$  (lower excitation potential), (ii) mean Fe I and Fe II abundances are equal, and (iii) Fe I abundances do not depend upon  $W_\lambda$ , while assuming that the LTE Saha–Boltzmann equation holds.

The measurement of  $W_\lambda$  for each Fe line (selected from the line list of Takeda et al. 2005) was done using the Gaussian-fitting method in most cases (though a special function constructed by convolving the rotational broadening function with the Gaussian function was used for several cases of appreciably large rotational velocity). In order to avoid measuring inadequate lines affected by blending, we carried out measurements on the computer display, while comparing the stellar spectrum with the Kurucz et al. (1984) solar

spectrum and examining the theoretical strengths of neighborhood lines computed with the help of Kurucz & Bell’s (1995) atomic line data.

In practice, we applied the program TGVIT (Takeda et al. 2005; see Section 2 therein), to the measured  $W_\lambda$  of the Fe I and Fe II lines. As done in Takeda et al. (2005), we restricted ourselves to using lines satisfying  $W_\lambda \leq 100$  mÅ, and those showing abundance deviations from the mean larger than  $2.5\sigma$  were rejected. The typical numbers of finally adopted lines are 72–235 (mean = 208) for Fe I and 5–22 (mean = 14) for Fe II (the number of available lines is smaller for stars showing broader lines). The resulting final parameters are presented in Table 1 and “tableE1.dat.” The internal statistical errors (see Section 3.2 of Takeda et al. 2002) involved with these solutions are in the range 10–85 K (mean = 24 K) for  $T_{\text{eff}}$ , 0.02–0.26 dex (mean = 0.06 dex) for  $\log g$ , 0.1–0.5  $\text{km s}^{-1}$  (mean = 0.2  $\text{km s}^{-1}$ ) for  $v_t$ , and 0.01–0.07 dex (mean = 0.03 dex) for [Fe/H]. The detailed data of  $W_\lambda$  and  $A(\text{Fe})$  (Fe abundances corresponding to the final solutions) for each star are given in “tableE2.dat” of the supplementary .tar.gz package.

#### 3.2. Trends and Mutual Correlations

These spectroscopically determined  $T_{\text{eff}}$  values are plotted against  $B - V$  and  $M_V$  in Figures 1(b) and (c), where we can see that they are well correlated with each other. The color-dependence of [Fe/H] depicted in Figure 1(d) indicates the near-constancy of [Fe/H] for Hyades stars and a tendency

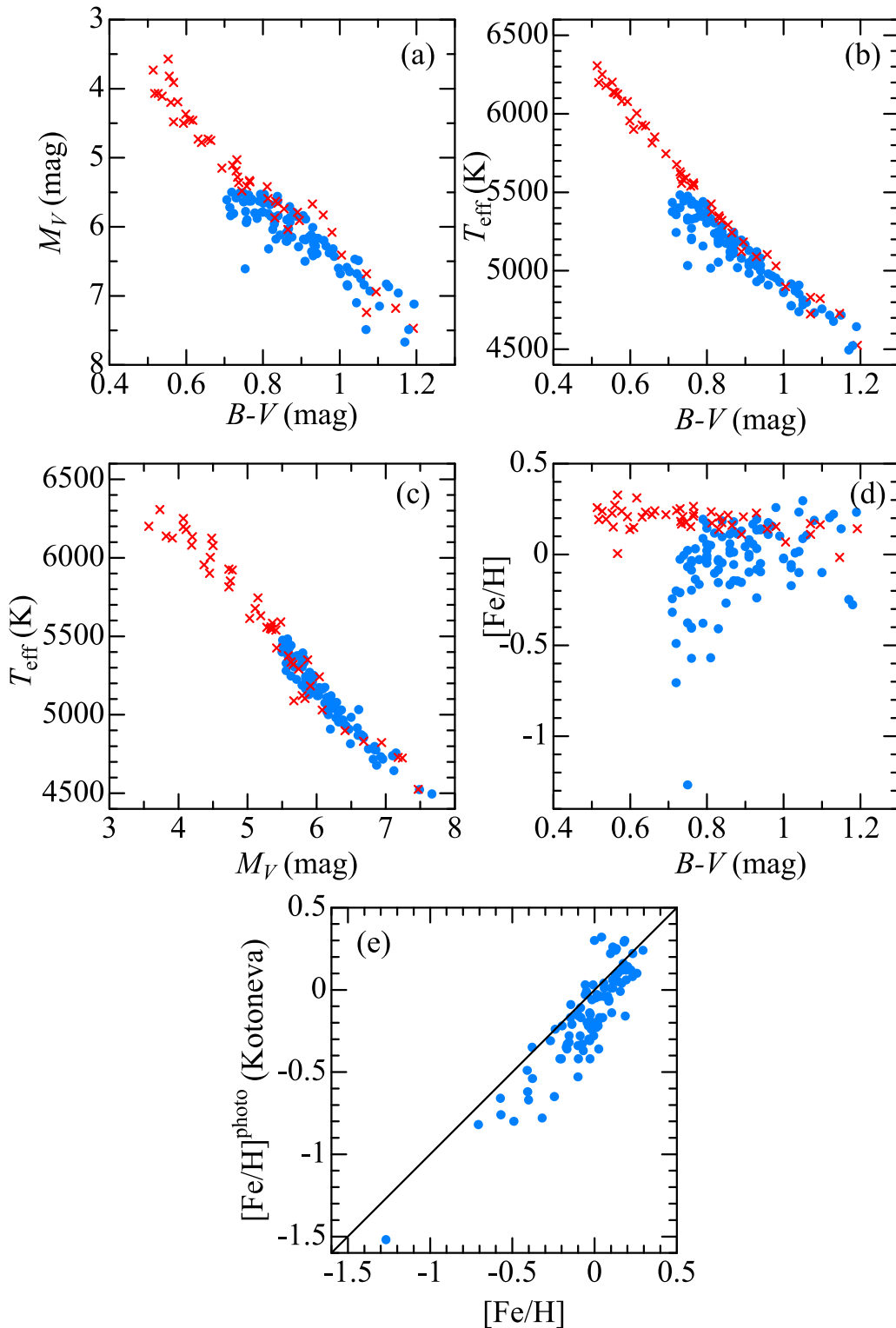


**Figure 1.** Panels (a)–(d): correlation diagram between the photometric data (absolute visual magnitude  $M_V$  and  $B - V$  color, mainly derived from the *Hipparcos* catalog) and the spectroscopically determined atmospheric parameters (see Section 3.1) of the program stars: (a)  $M_V$  vs.  $B - V$ , (b)  $T_{\text{eff}}$  vs.  $B - V$ , (c)  $T_{\text{eff}}$  vs.  $M_V$ , and (d)  $[\text{Fe}/\text{H}]$  vs.  $B - V$ . Panel (e) shows the interrelationship between the spectroscopic metallicity established in this study (abscissa) and the photometric metallicity ( $[\text{Fe}/\text{H}]^{\text{photo}}$ ) evaluated by Kotoneva et al. (2002) based on the position in the color–magnitude diagram (ordinate). Our program sample of 47 Hyades stars and 101 field stars are represented by red crosses and blue circles, respectively.

of decreasing  $[\text{Fe}/\text{H}]$  toward a bluer  $B - V$  for field stars (consistent with Figure 8 of Kotoneva et al. 2002). Figure 1(e) shows the comparison of our spectroscopic  $[\text{Fe}/\text{H}]$  with the photometric metallicity ( $[\text{Fe}/\text{H}]^{\text{photo}}$ )

determined by Kotoneva et al. based on the position in the color–magnitude diagram, which shows a reasonable correlation between these two (though their  $[\text{Fe}/\text{H}]^{\text{photo}}$  tends to be somewhat lower).

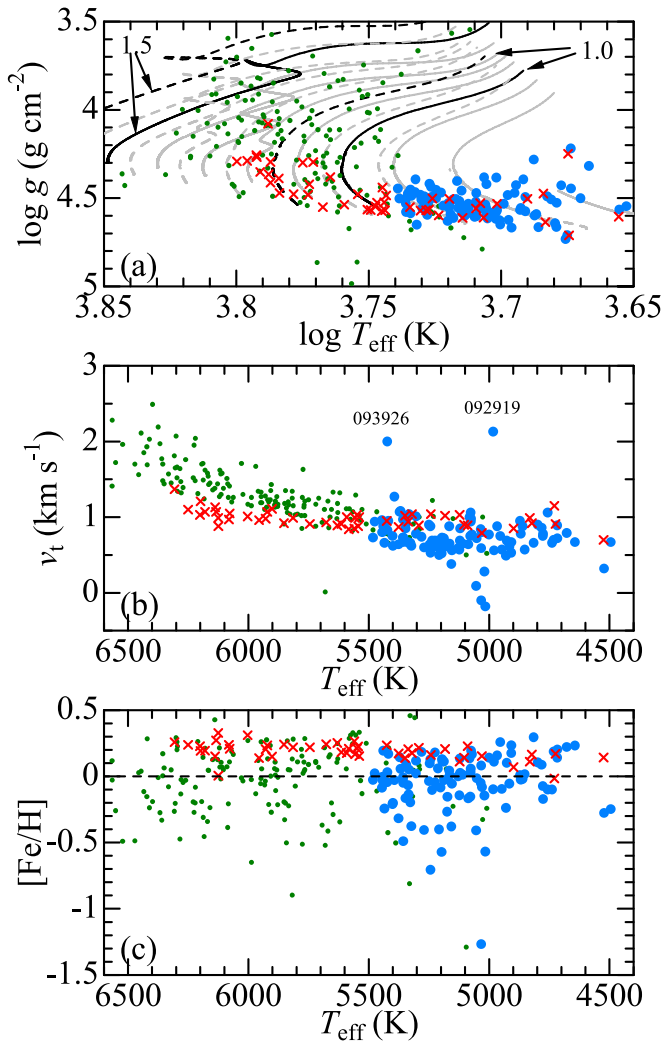


**Figure 2.** Spectroscopically determined  $\log g$ ,  $v_t$ , and  $[\text{Fe}/\text{H}]$  plotted against  $T_{\text{eff}}$  in panels (a), (b), and (c), respectively. In panel (a) are also depicted the theoretical  $\log g$  vs.  $\log T_{\text{eff}}$  relations corresponding to eight different masses (0.7, 0.8, 0.9, 1.0, 1.1, 1.2, 1.3, 1.4, and 1.5  $M_{\odot}$ ) for different metallicities ( $z = 0.01$  and  $z = 0.02$  as dashed and solid lines, respectively), which were taken from PARSEC stellar evolutionary tracks (Bressan et al. 2012, 2013). Apart from the program stars of this study (47 Hyades and 101 field stars shown by blue circles and red crosses respectively), 160 mid-F through early-K dwarfs/subgiants investigated by Takeda et al. (2005) are also plotted as green dots for comparison.

In Figures 2(a)–(c) are plotted  $\log g$ ,  $v_t$ , and  $[\text{Fe}/\text{H}]$  against  $T_{\text{eff}}$ , where the results of 160 dwarfs/subgiants (of mostly F–G type) determined by Takeda et al. (2005) are also shown for comparison. We can see from Figure 2(a) (where theoretical  $\log g$  versus  $\log T_{\text{eff}}$  relations are also depicted) that most of our program stars occupy consistent positions as main-sequence stars. However, deviations (i.e., underestimation of  $\log g$ ) begin to appear toward low- $T_{\text{eff}}$  end, which means that the precision of  $\log g$  tends to gradually deteriorate as  $T_{\text{eff}}$  is lowered below  $\lesssim 5000$  K. (see Section 5.1).

Regarding microturbulence, meaningless negative  $v_t$  values were obtained for two considerably metal-poor stars, HIP 057939 ( $-0.10$  km s $^{-1}$ ) and HIP 098792 ( $-0.18$  km s $^{-1}$ ), which are the result of extrapolation. In actual determination of oxygen abundance (see Section 4), we tentatively assigned  $v_t = 0.5$  km s $^{-1}$  for these stars. We also note that two stars (HIP 093926,

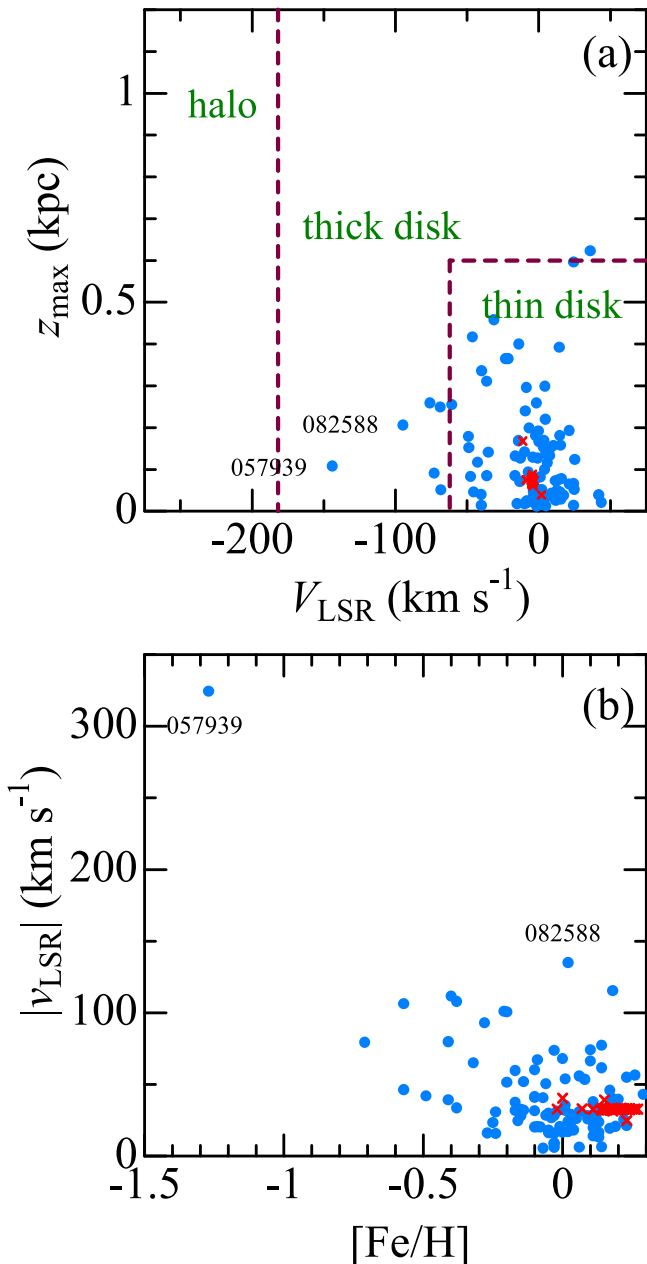
HIP 092919) show anomalously high  $v_t$  values ( $\sim 2$  km s $^{-1}$ ), which must be related to the fact that these stars show exceptionally broad lines indicative of higher rotation. It is interesting to note in Figure 2(b) that, while the  $v_t$  results determined for the 101 field stars (blue circles) tend to decrease as  $T_{\text{eff}}$  is lowered as a natural continuation of the trend derived by Takeda et al. (2005) (represented by green dots), those obtained for the 47 Hyades stars (red crosses) appear to be almost independent upon  $T_{\text{eff}}$  and nearly flat at  $\sim 1$  km s $^{-1}$ . This suggests the possibility that  $v_t$  could be in some way influenced by stellar age or activity, because Hyades stars are comparatively younger and of higher activity.

Figure 2(c) shows that the metallicities of Hyades stars are nearly constant at  $[\text{Fe}/\text{H}] \sim 0.2$ ; i.e., the mean ( $\pm$ standard deviation) is  $\langle [\text{Fe}/\text{H}] \rangle = 0.19 (\pm 0.07)$ . This is slightly higher than the value of  $\langle [\text{Fe}/\text{H}] \rangle = 0.11 (\pm 0.08)$  derived for F–G dwarfs by Takeda et al. (2013), but consistent within permissible limits in view of the fact that the published values of Hyades metallicity range over  $0.1 \lesssim [\text{Fe}/\text{H}] \lesssim 0.2$ .<sup>6</sup>

Meanwhile, values for field G–K stars range mostly from  $-0.7$  to  $+0.3$  (like the case of 160 sample stars studied by Takeda et al. 2005), though only HIP 057939 is distinctly metal-deficient ( $[\text{Fe}/\text{H}] = -1.27$ ) compared to the others. In connection with metallicity, it may be worth examining the population of our program stars. For this purpose, their kinematic parameters were computed following the same procedure as adopted in Takeda (2007; see Section 2.2 therein), where the necessary data (equatorial coordinates, parallax, proper motions, and radial velocity<sup>7</sup>) were taken from those of *Gaia* DR2 (Gaia Collaboration et al. 2016, 2018) published as CDS/ADC Collection of Electronic Catalogues (No. 1345, 0, 2018) and available via SIMBAD. The resulting orbital parameters and space velocity components relative to the local standard of rest (LSR) are given in tableE1.dat of the supplementary .tar.gz package. The  $z_{\text{max}}$  (maximum separation from the Galactic plane) versus  $V_{\text{LSR}}$  (rotation velocity component) diagram usable for discriminating stellar population is displayed in Figure 3(a), which indicates that most of our target stars belong to the thin disk population (with a few exceptions such as HIP 057939 and HIP 082588 which may be from the thick-disk population). Figure 3(b) illustrates the correlation between the space velocity  $|v_{\text{LSR}}| (\equiv \sqrt{U_{\text{LSR}}^2 + V_{\text{LSR}}^2 + W_{\text{LSR}}^2})$ , and metallicity ( $[\text{Fe}/\text{H}]$ ). Though the scatter is rather large, we can recognize that  $|v_{\text{LSR}}|$  tends to increase with a decrease in  $[\text{Fe}/\text{H}]$  as expected. It can also be seen that those two stars from the apparent thick-disk population mentioned above show distinctly larger  $|v_{\text{LSR}}|$  (especially HIP 057939).

<sup>6</sup> Takeda (2008) summarized the Hyades  $[\text{Fe}/\text{H}]$  values determined by 13 spectroscopic studies in 1971–2005 (see Figure 32.8(a) therein), which are between  $+0.1$  and  $+0.2$  (the mean is  $+0.14$  with a standard deviation of 0.03). The same argument almost holds for the more recent literature values, as summarized in Section 5.5 of Dutra-Ferreira et al. (2016), who themselves derived two values of  $+0.18 \pm 0.03$  (using well-constrained parameters) and  $+0.14 \pm 0.03$  (classical method) for the average  $[\text{Fe}/\text{H}]$  value of dwarfs +giants in the Hyades cluster.

<sup>7</sup> We found that *Gaia* DR2 heliocentric radial velocities are consistent with those measured from our spectra for most of our program stars. The exceptions (showing differences more than 3 km s $^{-1}$ ) are HIP 093926 ( $-37.9$ ), HIP 013891 ( $+13.5$ ), HIP 040419 ( $-7.9$ ), HIP 104214 ( $+6.3$ ), HIP 012158 ( $-5.7$ ), and HIP 092919 ( $-4.7$ ), where the parenthesized values are  $V_{\text{rad}}^{\text{hel}}(\text{Gaia}) - V_{\text{rad}}^{\text{hel}}(\text{ours})$  (in km s $^{-1}$ ). These stars are likely to be spectroscopic binaries.



**Figure 3.** (a) Correlation diagram between the maximum separation from the Galactic plane ( $z_{\max}$ ) and the rotation velocity component relative to the local standard of rest ( $V_{\text{LSR}}$ ), which may be used for classifying the stellar population (the boundaries are indicated by the dashed lines; see Ibukiyama & Arimoto 2002). (b) Space velocity relative to the local standard of rest  $|v_{\text{LSR}}| \equiv (U_{\text{LSR}}^2 + V_{\text{LSR}}^2 + W_{\text{LSR}}^2)^{1/2}$  plotted against  $[\text{Fe}/\text{H}]$ . Symbols have the same meanings as in Figure 1.

## 4. Oxygen Abundance Determination

### 4.1. Spectrum-fitting Analysis

We determine the oxygen abundances of 148 target stars from the O I 7771–5 triplet feature as done in previous studies (e.g., Takeda et al. 2015). Based on the atmospheric parameters determined in Section 3.1, the model atmosphere for each star was constructed by interpolating the Kurucz (1993) ATLAS9 model grid. We similarly evaluated the non-LTE departure coefficients for O corresponding to each model by interpolating the grid computed by Takeda (2003).

Abundance determination was carried out using the spectrum-fitting technique as done in Takeda et al. (2015), which establishes the optimum solutions giving the best match between theoretical and observed spectra using the numerical algorithm described in Takeda (1995), while simultaneously varying the abundances of relevant key elements ( $A_1, A_2, \dots$ ), the macrobroadening parameter ( $v_M$ ),<sup>8</sup> and the radial-velocity (wavelength) shift ( $\Delta\lambda$ ).

We selected 7770–7782 Å as the wavelength region for fitting, which includes the O I 7771–5 triplet lines and Fe I 7780 line as the conspicuous lines. Regarding the atomic data of spectral lines, the same values as used in Takeda et al. (2015) were used unchanged for three lines of the O I 7771–5 triplet and six lines of CN molecules (see Table 2 therein). Otherwise, we invoked the data compiled in the VALD database (Ryabchikova et al. 2015) for all lines included in this region (for example,  $\log gf = +0.03$  was adopted for the strong Fe I 7780.556 line of  $\chi_{\text{low}} = 4.47$  eV). We varied only  $A(\text{O})$  and  $A(\text{Fe})$  for the abundances to be adjusted, while other elemental abundances (necessary for computing the background spectrum in this region) were fixed at the metallicity-scaled values.<sup>9</sup> The non-LTE effect was taken into account for the O I 7771–5 lines. Since the OAO/HIDES spectrum often suffers defects due to bad columns of CCD in this region, we had to mask them occasionally. The convergence of the solutions turned out fairly successful for all cases. How the theoretical spectrum for the converged solutions fits well with the observed spectrum for each star is displayed in Figure 4 (Hyades stars) and Figure 5 (field stars).

### 4.2. Abundance-related Quantities

Next, with the help of the Kurucz (1993) WIDTH9 program (which had been considerably modified in various respects; e.g., inclusion of non-LTE effects, etc.), we computed the equivalent widths ( $W_{7772}$ ,  $W_{7774}$ , and  $W_{7775}$ ) of three O I triplet lines (at 7771.944, 7774.166, and 7775.388 Å) inversely from the non-LTE abundance solution  $A^{\text{N}}(\text{O})$  (resulting from fitting analysis) along with the adopted atmospheric model and parameters. Based on these  $W$  values, the non-LTE ( $A^{\text{N}}$ : essentially the same as the fitting solution) and LTE ( $A^{\text{L}}$ ) oxygen abundances were then derived, from which the corresponding non-LTE corrections could be obtained as  $\Delta \equiv A^{\text{N}} - A^{\text{L}}$ . In Table 1 (and also in “tableE1.dat”) are presented  $[\text{O}/\text{H}] \equiv A^{\text{N}} - 8.861$ ,<sup>10</sup>  $W_{7774}$ ,  $\Delta_{7774}$  (for the middle line of the triplet).

<sup>8</sup> This  $v_M$  is the  $e$ -folding half-width of the Gaussian broadening function ( $\propto \exp[-(v/v_M)^2]$ ), which represents the combined broadening width of instrumental profile, macroturbulence, and rotational velocity.

<sup>9</sup> Although the abundances of CN and Nd were also varied (in addition to O and Fe) in Takeda et al. (2015), we decided to fix them in this study, because these line features are less significant for dwarfs compared to the case of giants. Note also that, since the role of  $A(\text{Fe})$  is a fudge parameter to accomplish the satisfactory fit for the whole region, its solution was not used for deriving  $[\text{Fe}/\text{H}]$  of a star, for which we adopted the value determined from many Fe lines (see Section 3.1).

<sup>10</sup> Regarding the solar oxygen abundance, Takeda et al. (2015) derived  $A_{\odot}^{\text{N}} = 8.861$  (in the usual normalization of  $A(\text{H}) = 12.00$ ) as the non-LTE solar oxygen abundance with  $\Delta_{7774} = -0.102$  and  $W_{7774} = 63.2$  mÅ. This solar  $A_{\odot}^{\text{N}}$  is the value obtained in the same manner as adopted in this analysis (e.g., same line parameters, etc.), which is necessary to accomplish the purely differential analysis for  $[\text{O}/\text{H}]$ . Although its absolute value is apparently larger than the recent solar oxygen abundance of 8.69 (Asplund 2009) and rather near to the old one (e.g., 8.83 by Grevesse & Sauval 1998), this difference does not matter here.

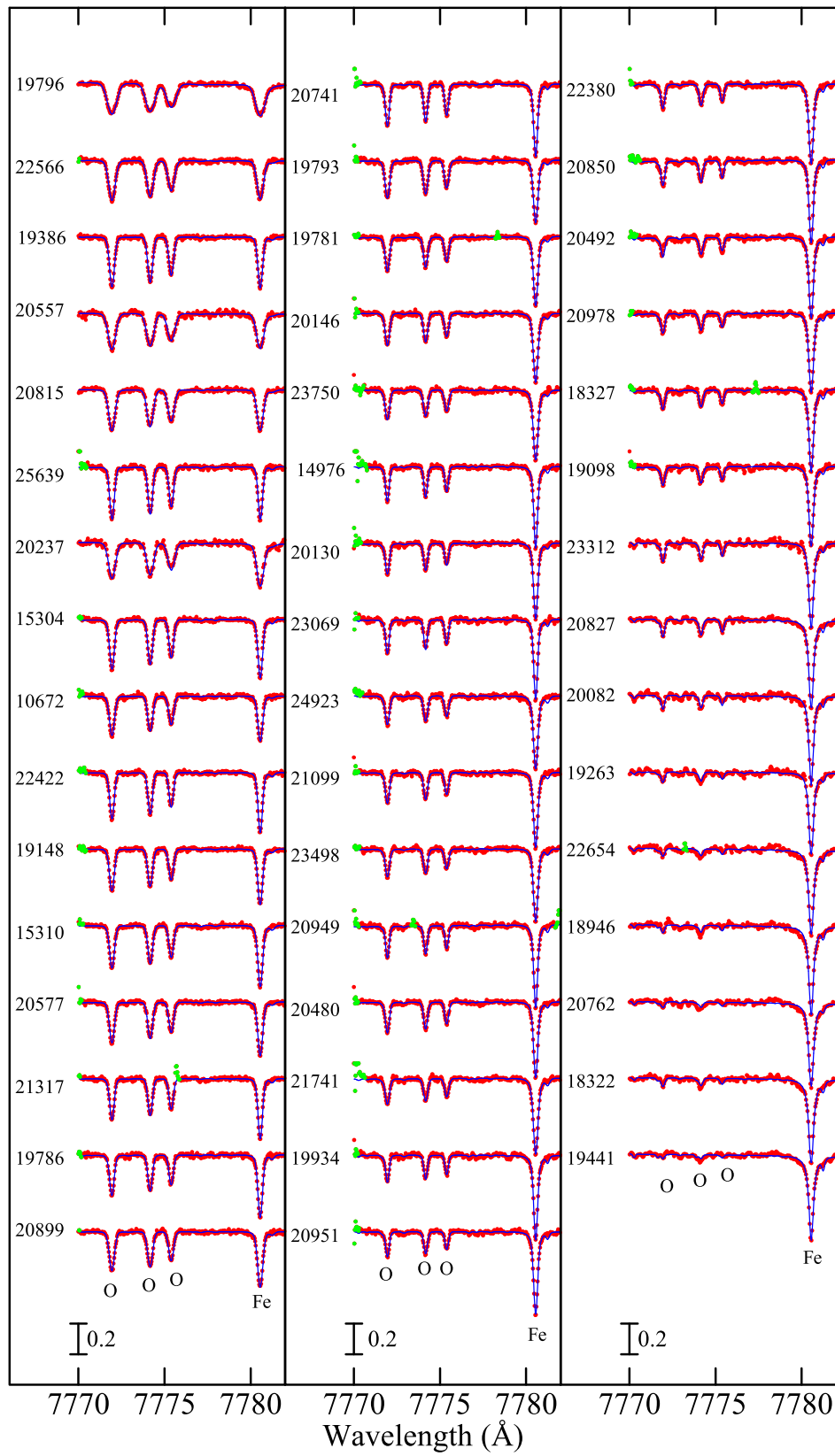


**Figure 4.** Synthetic spectrum fitting in the 7770–7782 Å region comprising the O I 7771–5 and Fe I 7780 lines for the 47 Hyades stars. The best-fit theoretical spectra are shown as dark blue solid lines. The observed data used in the fitting are plotted as red symbols, while those rejected in the fitting (e.g., due to spectrum defect) are highlighted in green. In each panel (from left to right), the spectra are arranged in descending order of  $T_{\text{eff}}$  as in Table 1, and vertical offsets of 0.5 are applied to each spectrum (indicated by the HIP number) relative to the adjacent one. The wavelength scale is adjusted to the laboratory frame by correcting the stellar radial velocity.

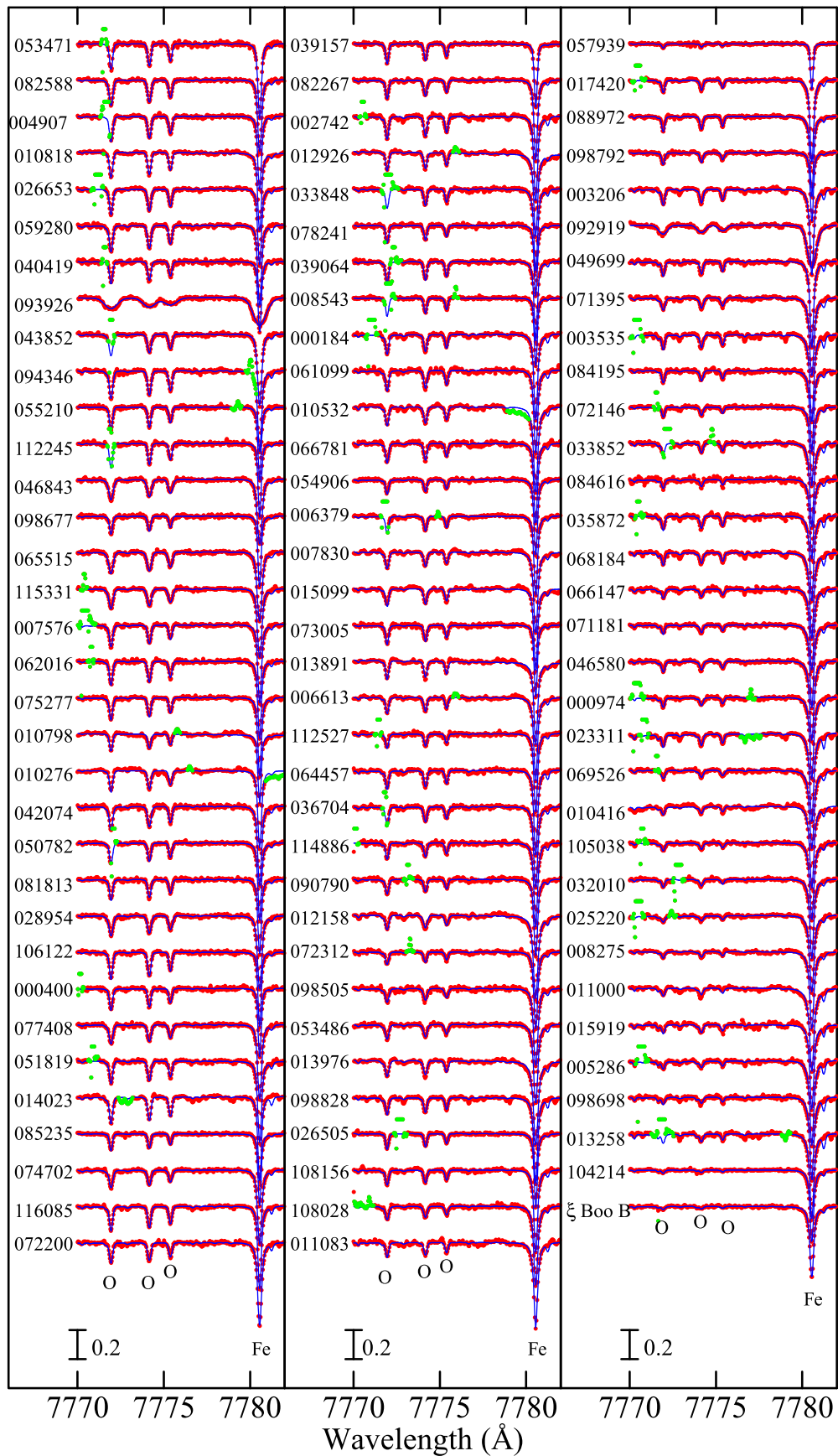


**Figure 5.** Synthetic spectrum fitting in the 7770–7782 Å region for the 101 field stars. A vertical offset of 0.25 is applied to each spectrum relative to the adjacent one. Plot color details are the same as in Figure 4.

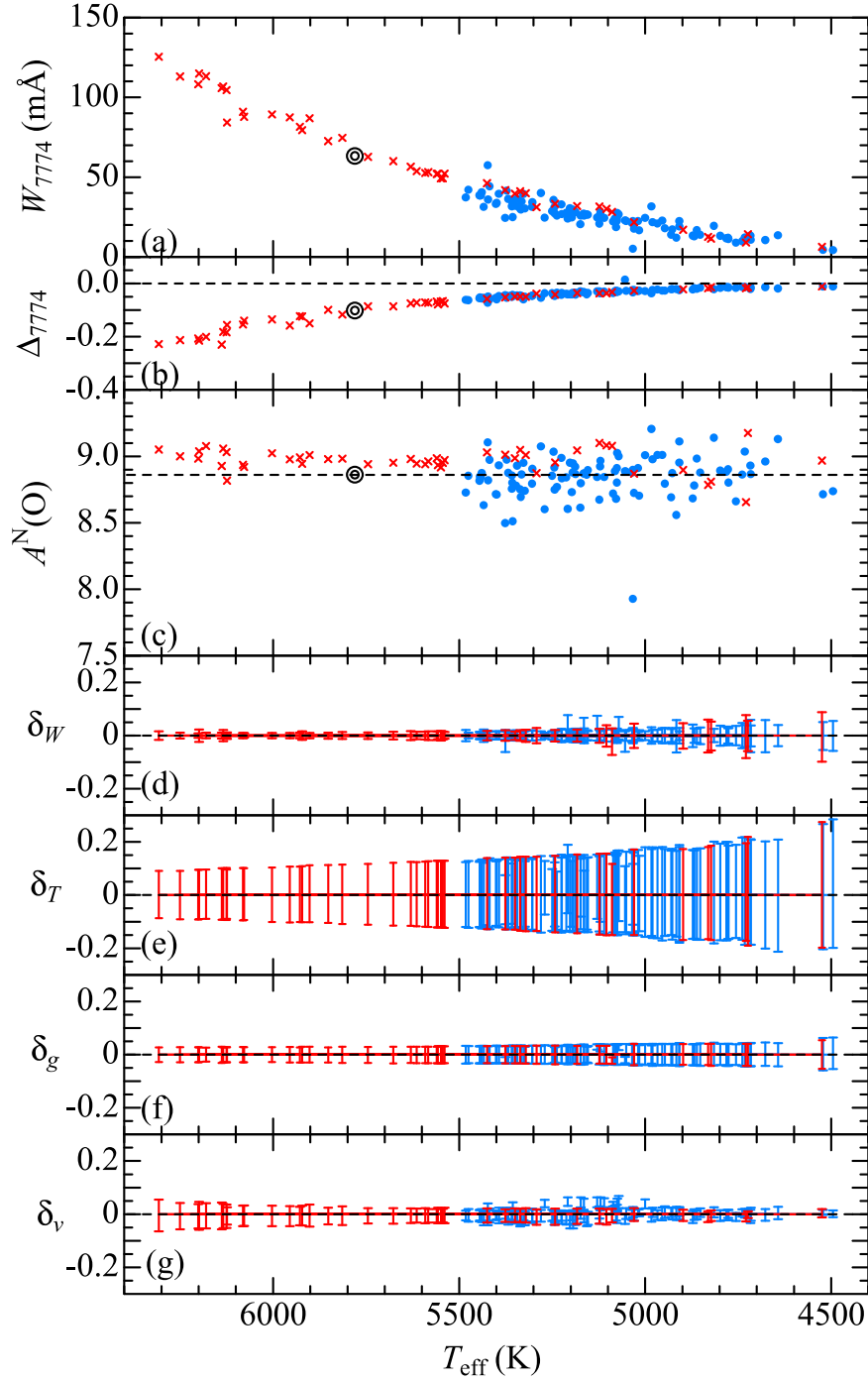


**Figure 6.** Oxygen abundance and related quantities plotted against  $T_{\text{eff}}$ . (a)  $W_{7774}$  (equivalent width of O I 7774.166), (b)  $\Delta_{7774}$  (non-LTE correction for O I 7774.166), (c)  $A^{\text{N}}(\text{O})$  (non-LTE oxygen abundance derived from spectrum fitting). (d)  $\delta_{W+}$  and  $\delta_{W-}$  (abundance change corresponding to perturbation of  $+\delta W$  and  $-\delta W$ , where  $\delta W$  is the uncertainty of equivalent width evaluated according to Cayrel 1988). (e)  $\delta_{T+}$  and  $\delta_{T-}$  (abundance variations in response to  $T_{\text{eff}}$  changes of  $+100$  and  $-100$  K), (f)  $\delta_{g+}$  and  $\delta_{g-}$  (abundance variations in response to  $\log g$  changes by  $+0.1$  and  $-0.1$  dex), and (g)  $\delta_{v+}$  and  $\delta_{v-}$  (abundance variations in response to perturbing the  $v_t$  value by  $+0.5$  and  $-0.5$   $\text{km s}^{-1}$ ). Note that the signs of these  $\delta$  values are  $\delta_{W+} > 0$ ,  $\delta_{W-} < 0$ ,  $\delta_{T+} < 0$ ,  $\delta_{T-} > 0$ ,  $\delta_{g+} > 0$ ,  $\delta_{g-} < 0$ ,  $\delta_{v+} < 0$ , and  $\delta_{v-} > 0$ . The non-LTE solar O abundance of 8.861 derived in a similar manner (see Takeda et al. 2015) is indicated by the horizontal dashed line in panel (c). The large double circles in panels (a)–(c) denote the solar values (see footnote 10). Meanings of the symbols (and their colors) are as in Figure 1.

In order to estimate abundance errors caused by uncertainties in atmospheric parameters, we derived six kinds of abundance variations ( $\delta_{T+}$ ,  $\delta_{T-}$ ,  $\delta_{g+}$ ,  $\delta_{g-}$ ,  $\delta_{v+}$ , and  $\delta_{v-}$ ) for  $A^{\text{N}}$  by repeating the analysis on the  $W_{7774}$  values while perturbing the standard atmospheric parameters interchangeably by  $\pm 100$  K in  $T_{\text{eff}}$ ,  $\pm 0.1$  dex in  $\log g$ , and  $\pm 0.5$   $\text{km s}^{-1}$  in  $v_t$  (which are larger than

the internal statistical errors described in Section 3.1 but tentatively chosen by considering possible systematic errors; see Section 5.1).

Errors ( $\delta W$ ) due to random noise in the equivalent widths ( $W$ ) were also estimated by invoking the relation derived by Cayrel (1988) corresponding to S/N ( $\sim 100$ – $200$ ) measured for

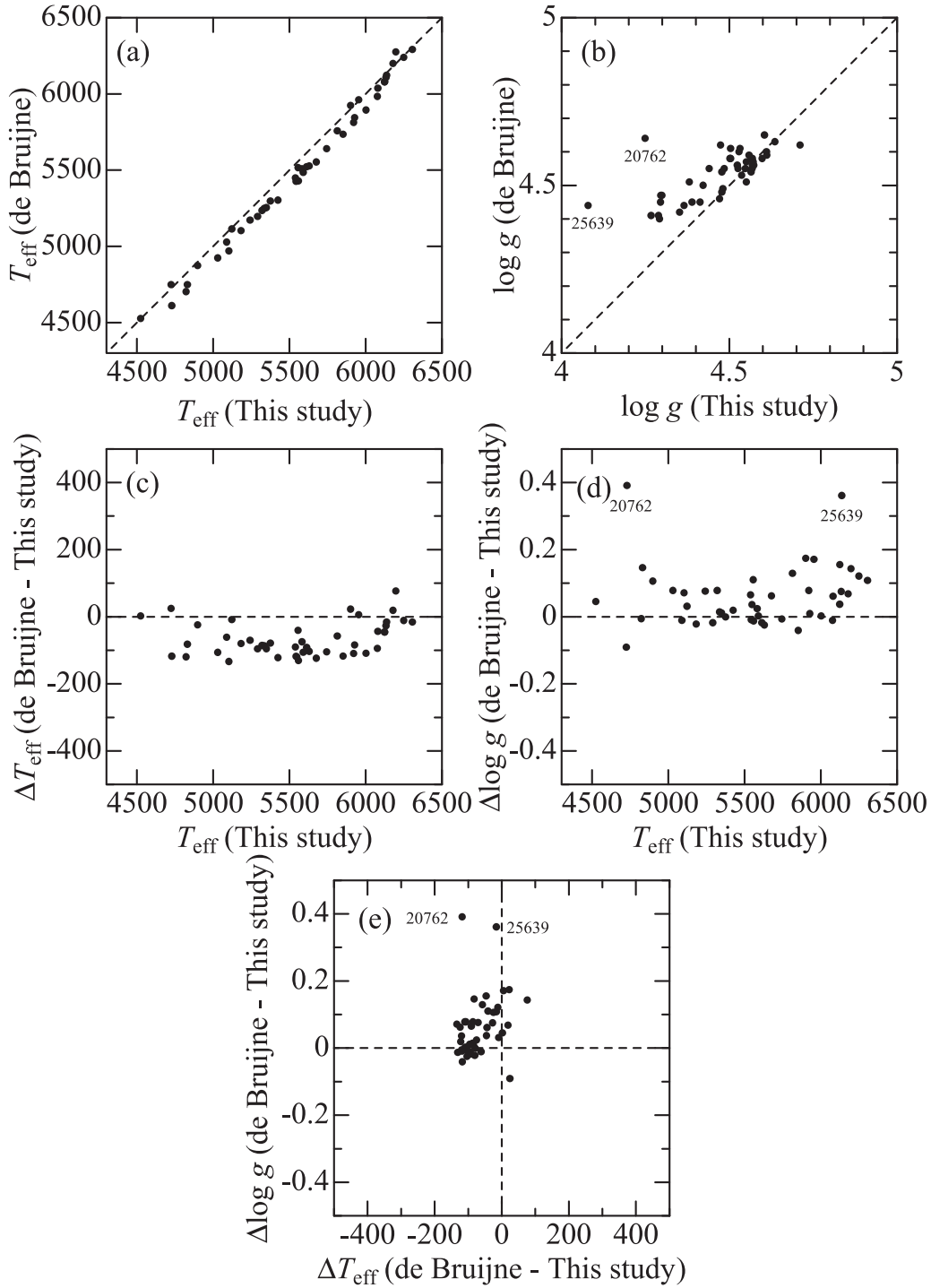


**Figure 7.** Comparison of the  $T_{\text{eff}}$  and  $\log g$  values determined for the Hyades stars in this study (based on Fe I and Fe II lines) with those of de Bruijne et al. (2001) (all of our 47 Hyades stars are included their sample). (a)  $T_{\text{eff}}$  (theirs) vs.  $T_{\text{eff}}$  (ours), (b)  $\log g$  (theirs) vs.  $\log g$  (ours), (c)  $\Delta T_{\text{eff}}$  (theirs–ours) vs.  $T_{\text{eff}}$  (ours), (d)  $\Delta \log g$  (theirs–ours) vs.  $\log g$  (ours), and (e)  $\Delta \log g$  (theirs–ours) vs.  $\Delta T_{\text{eff}}$  (theirs–ours).

each star’s spectrum in the neighborhood of the O I triplet. We then evaluated the abundances for each of the perturbed  $W_+$  ( $\equiv W + \delta W$ ) and  $W_-$  ( $\equiv W - \delta W$ ), from which the differences from the standard abundance ( $A$ ) were derived as  $\delta_{W_+}$  ( $>0$ ) and  $\delta_{W_-}$  ( $<0$ ).

These  $W_{7774}$ ,  $\Delta_{7774}$ ,  $A^N(\text{O})$ ,  $\delta_{W_{\pm}}$ ,  $\delta_{T_{\pm}}$ ,  $\delta_{g_{\pm}}$ , and  $\delta_{v_{\pm}}$  are plotted against  $T_{\text{eff}}$  in panels (a)–(g) of Figure 6, respectively, from which the following trends can be read.

1. It can be seen that  $W_{7774}$  progressively decreases as  $T_{\text{eff}}$  is lowered, reflecting that the occupation number in the highly excited lower level ( $\chi_{\text{low}} = 9.15$  eV) of this transition is quite  $T_{\text{eff}}$ -sensitive ( $\propto 10^{-5040\chi_{\text{low}}/T_{\text{eff}}}$ ).
2. Likewise,  $|\Delta_{7774}|$  (absolute value of negative non-LTE correction) declines with decreasing  $T_{\text{eff}}$ , because of the close connection between  $\Delta$  and  $W$  (see Takeda 2003) for the O I 7771–5 triplet. Accordingly, while the non-LTE

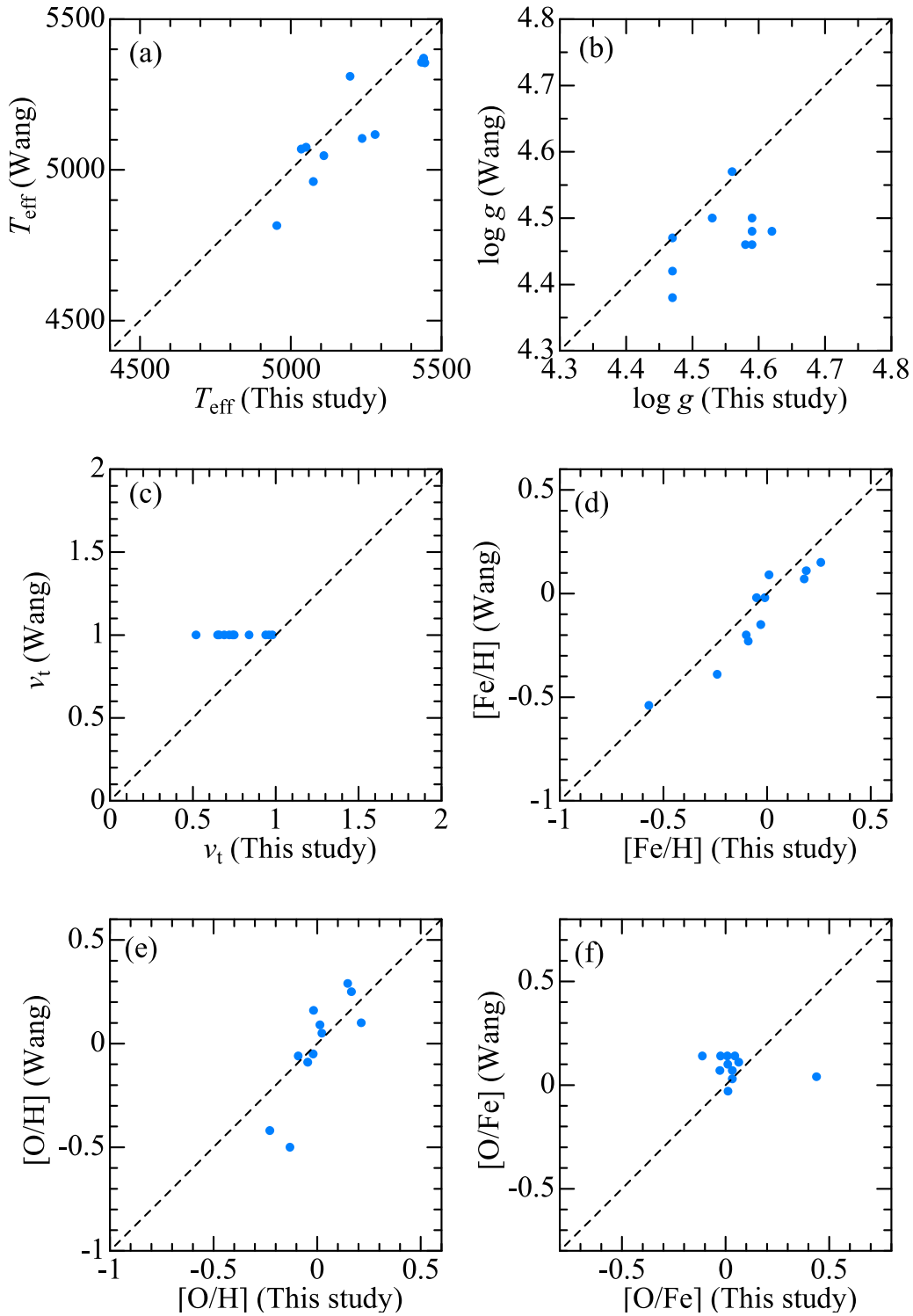


**Figure 8.** Comparison of the atmospheric parameters and the oxygen abundances derived in this study with those of Wang et al. (2009) for 11 field stars in common. (a)  $T_{\text{eff}}$ , (b)  $\log g$ , (c)  $v_t$ , (d)  $[\text{Fe}/\text{H}]$ , (e)  $[\text{O}/\text{H}]$ , and (f)  $[\text{O}/\text{Fe}]$ . (Note that they assumed  $v_t = 1 \text{ km s}^{-1}$ .)

correction is still appreciable for late F–early G dwarfs ( $\sim 0.1$ – $0.2$  dex), it becomes practically negligible for K dwarfs at  $T_{\text{eff}} \lesssim 5000 \text{ K}$ .

3. The oxygen abundances ( $A^{\text{N}}$ ) do not show any clear  $T_{\text{eff}}$ -dependence for either Hyades or field stars. While the former are nearly constant on average (though the scatter

grows at  $T_{\text{eff}} \lesssim 5000 \text{ K}$ ), the latter are diversified mostly in the range of  $\sim 8.5$ – $9.2$ .

4. The mean of  $[\text{O}/\text{H}]$  for the 47 Hyades stars is  $\langle [\text{O}/\text{H}] \rangle = 0.11 (\pm 0.09)$ . Although this is slightly lower than the value ( $\langle [\text{O}/\text{H}] \rangle = 0.22 \pm 0.14$ ) derived by Takeda et al. (2013) for Hyades F–G dwarfs from O I

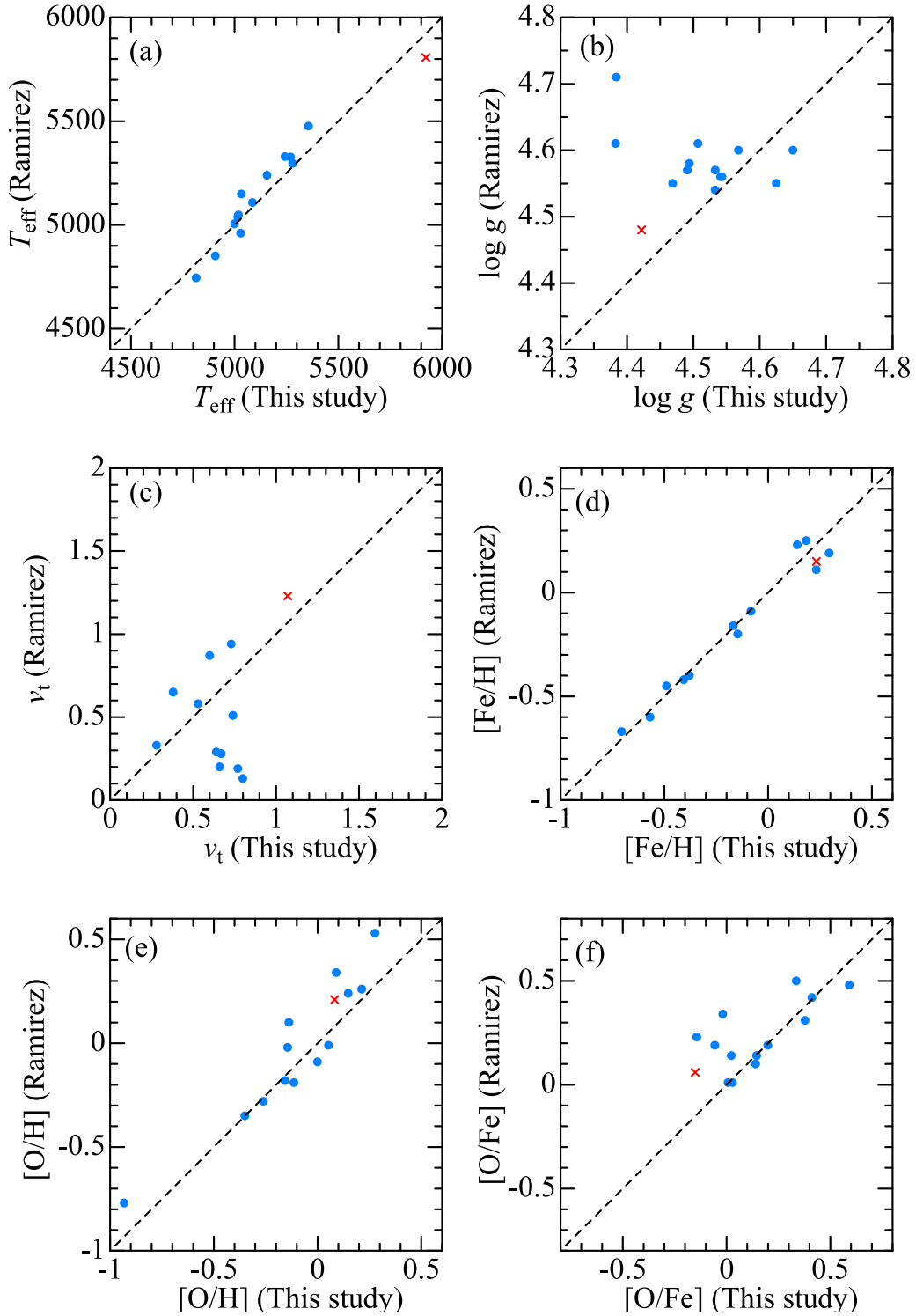


**Figure 9.** Comparison of the atmospheric parameters and the oxygen abundances derived in this study with those of Ramirez et al. (2013) for 13 field stars and one Hyades star in common. Parameters plotted as in Figure 8.

6156–8 lines, we consider that both are reasonably consistent within the allowable range (see Section 1 of Takeda et al. 2013 for a summary of published [O/H] values in the literature).

5. Among the various sources of abundance errors, most important is  $\delta_{T_{\pm}}$  (ranging from  $\sim 0.1$  dex to  $\sim 0.2$  dex or even more; especially large around lowest  $T_{\text{eff}}$ ) reflecting the high-excitation nature of O I triplet lines, while  $\delta_{W_{\pm}}$ ,

$\delta_{g_{\pm}}$  and  $\delta_{v_{\pm}}$  are comparatively insignificant (only several hundredths dex).

## 5. Discussion

### 5.1. Reliability of Spectroscopic Parameters

As to whether the stellar parameters of K dwarfs can be reliably determined based on Fe I and Fe II lines, which was

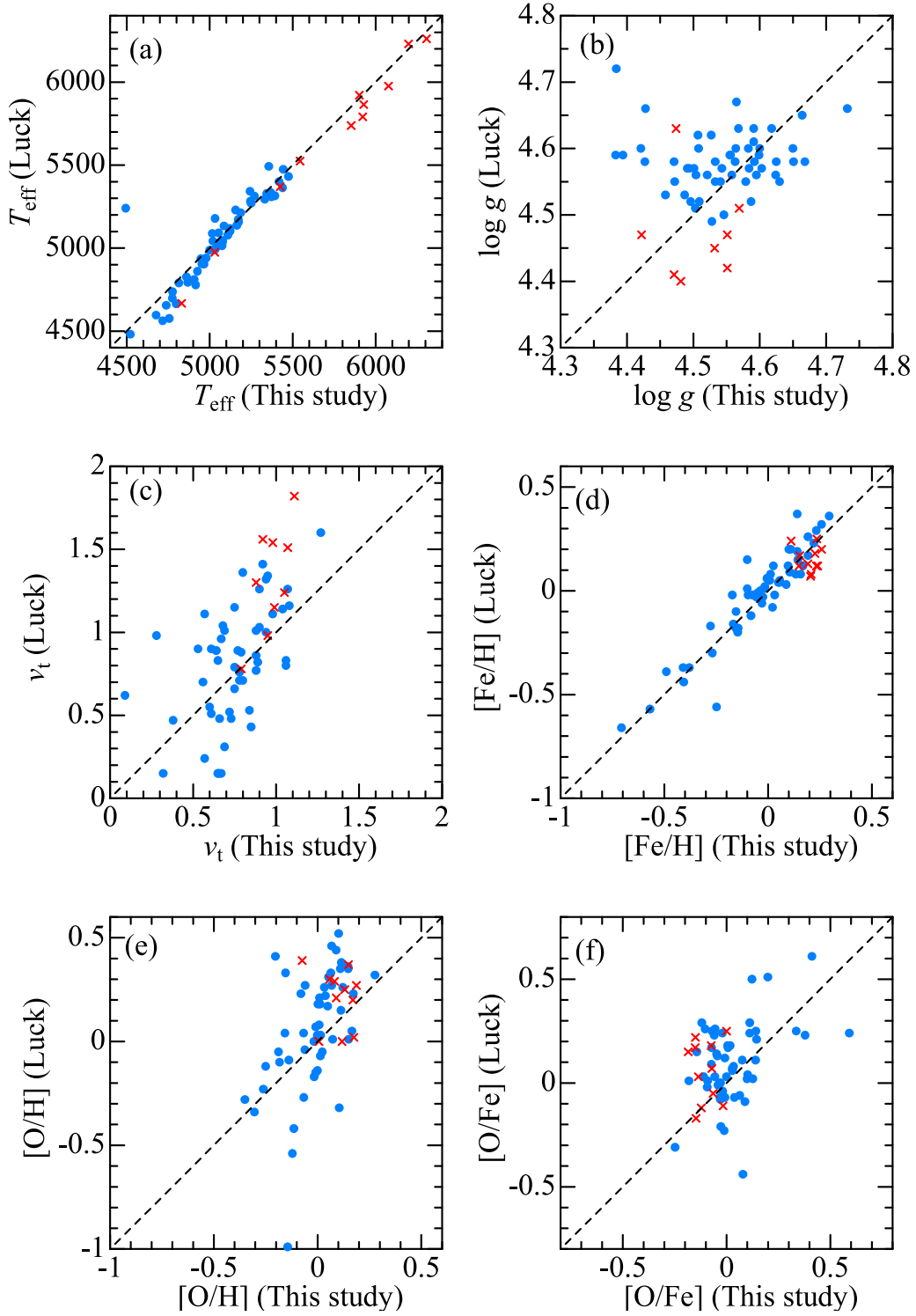


**Figure 10.** Comparison of the atmospheric parameters and the oxygen abundances derived in this study with those of Luck (2017) for 55 field stars and 11 Hyades stars in common. Parameters plotted as in Figure 8.

the first aim of this study (under the suspicion that LTE ionization equilibrium of Fe I/Fe II may break down), we can examine this problem by comparing the  $T_{\text{eff}}$  and  $\log g$  values of Hyades dwarfs spectroscopically derived in Section 3.1 with those of de Bruijne et al. (2001), who made use of the theoretical color–magnitude relations along with the well-established luminosities from *Hipparcos* parallaxes. These comparisons are illustrated in Figure 7.

Figure 7(a) suggests that a satisfactory agreement is observed for  $T_{\text{eff}}$ , though  $T_{\text{eff}}$  (this study) tends to be slightly higher than  $T_{\text{eff}}$  (de Bruijne et al.) by  $\lesssim 100$  K (Figure 7(c)). The average  $\langle \Delta T_{\text{eff}} \text{ (de Bruijne et al.} - \text{this study)} \rangle$  is  $-67 (\pm 50)$  K. Regarding  $\log g$ , we can see a tendency of  $\log g$  (this study) being smaller than  $\log g$  (de Bruijne et al.) (Figure 7(b)). However, excepting two stars (HIP 20762 and HIP 25639), the difference is within  $\lesssim 0.1\text{--}0.2$  dex (Figure 7(d)). The average

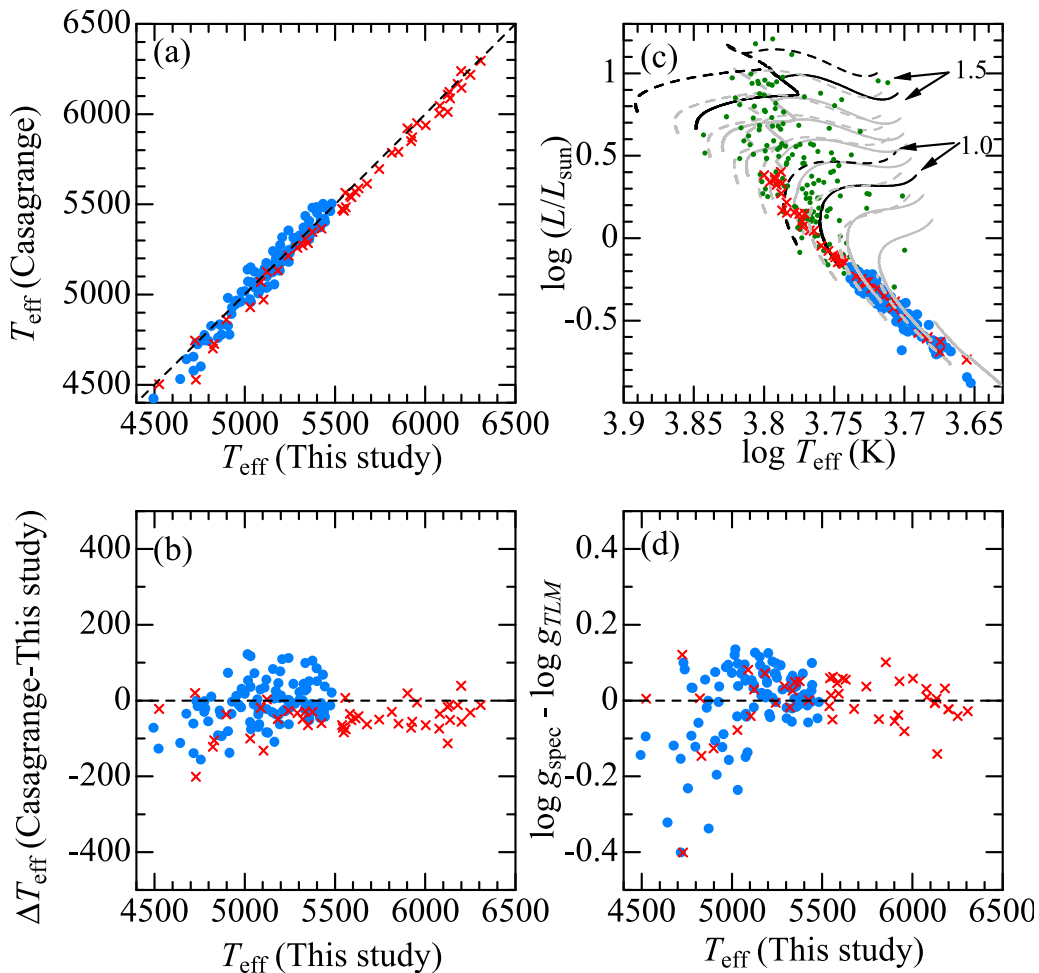


**Figure 11.** Panels (a) and (b): comparison of the photometric  $T_{\text{eff}}$  derived from  $B - V$  and  $[\text{Fe}/\text{H}]$  using the Casagrande et al. (2010) formula with the spectroscopic  $T_{\text{eff}}$  adopted in this study: (a)  $T_{\text{eff}}$  (Casagrande et al.) vs.  $T_{\text{eff}}$  (this study) and (b)  $T_{\text{eff}}$  (Casagrande et al.)  $- T_{\text{eff}}$  (this study) vs.  $T_{\text{eff}}$  (this study). Panel (c):  $L$  (bolometric luminosity) vs.  $T_{\text{eff}}$  relation for the program stars, where the theoretical PARSEC tracks are also depicted similarly to Figure 2(a). The differences between  $\log g_{\text{spec}}$  (spectroscopic surface gravity adopted in this study) and  $\log g_{\text{TLM}}$  (theoretical surface gravity derived from  $T_{\text{eff}}$ ,  $L$ , and  $M$ ) are plotted against  $T_{\text{eff}}$  in panel (d). See the caption of Figure 2 for the meanings of the symbols and lines.

$(\Delta \log g \text{ (de Bruijne} - \text{This study)})$  is  $+0.06 (\pm 0.09)$  dex (for all stars) or  $+0.05 (\pm 0.06)$  dex (excluding the two outliers). These  $\Delta T_{\text{eff}}$  and  $\Delta \log g$  show a weak correlation (Figure 7(e)) which is presumably because higher  $T_{\text{eff}}$  (enhancing ionization) is compensated by higher  $\log g$  (suppressing ionization).

Considering the results of this test using Hyades G–K stars, we may conclude that our spectroscopically determined  $T_{\text{eff}}$  and  $\log g$  do not suffer significant errors, which are determinable based on Fe I and Fe II lines to typical precisions of  $\lesssim 100$  K and  $\lesssim 0.1$  dex under the assumption of the LTE Saha–Boltzmann equation. Admittedly, the tendency of slightly higher  $T_{\text{eff}}$  and lower  $\log g$  in our spectroscopic parameters may indicate the possibility of marginal overionization. However, since  $\Delta T_{\text{eff}}$  as well as  $\Delta \log g$  do not show any conspicuous dependence upon  $T_{\text{eff}}$ , we can rule out the possibility of significant  $T_{\text{eff}}$ -dependent Fe I–Fe II discrepancy progressively increasing toward lower  $T_{\text{eff}}$ . In this regard, our result is in favor of Aleo et al.’s (2017) conclusion that this previously alleged considerable discordance between Fe I and Fe II abundances in K dwarfs is largely due to improper inclusion of blended Fe II lines and practically insignificant ( $\lesssim 0.1$  dex) as long as stars of  $T_{\text{eff}} \gtrsim 4500$  K are concerned. We should note, however, that lowering of the precision is more or less

unavoidable at the low  $T_{\text{eff}}$  regime (see Section 3.2 in connection with the trend of  $\log g$  versus  $T_{\text{eff}}$  in Figure 2(a)), because Fe II lines are so weakened that their measurements must suffer larger uncertainties.

It may be worth comparing the spectroscopic parameters with those determined by other methods in recent representative studies. Comparisons with the results of Wang et al. (2009), Ramírez et al. (2013), and Luck (2017) are shown in Figures 8, 9, and 10, respectively. In all three investigations,  $T_{\text{eff}}$  was determined photometrically from colors,  $\log g$  by comparing the position on the  $\log L$  versus  $\log T_{\text{eff}}$  diagram ( $L$ : stellar luminosity) with stellar evolutionary tracks, and  $v_t$  by requiring that the resulting abundances from Fe I lines do not show any systematic correlation with line strengths (though  $v_t = 1 \text{ km s}^{-1}$  was assumed by Wang et al. 2009). We can read the following characteristic trends from these figures.

1. Our spectroscopic  $T_{\text{eff}}$  is satisfactorily consistent with the photometrically determined values of all three studies (Figure 8(a), 9(a), and 10(a)<sup>11</sup>).

<sup>11</sup> One exceptional disagreement is that our  $T_{\text{eff}}$  (4495 K) for  $\xi$  Boo B or HD 131156B is considerably discrepant from Luck’s (2017) value (5240 K). We suspect that something was wrong in his derivation (e.g., adoption of the merged color of A+B?), because it is too high for a K5V star.

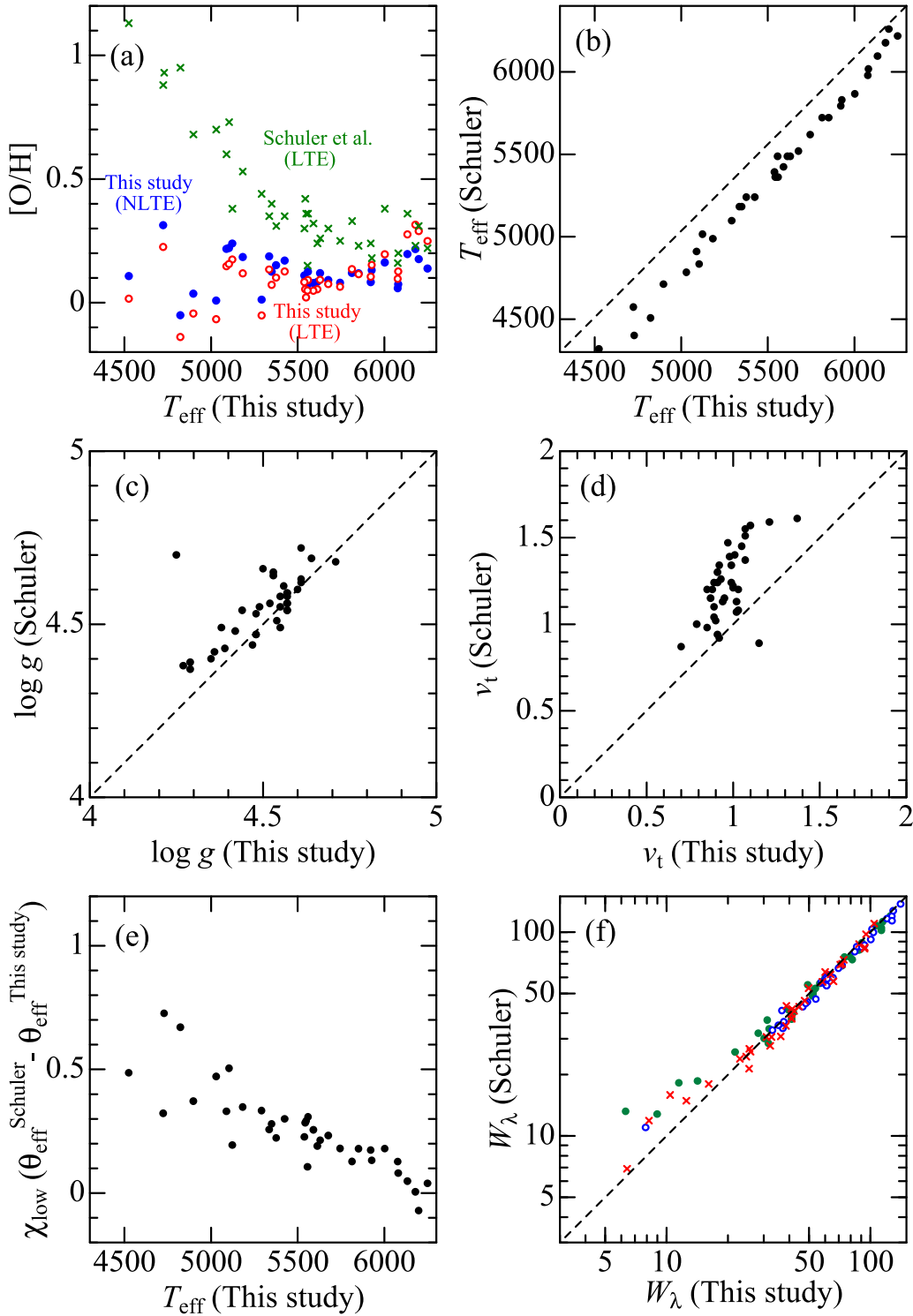


**Figure 12.** Comparison of the our oxygen abundances and atmospheric parameters derived for Hyades stars with those of Schuler et al. (2006b) (37 stars are in common). (a)  $[O/H]$  values plotted against  $T_{\text{eff}}$  (ours), where  $[O/H]$ (theirs, LTE),  $[O/H]$ (ours, NLTE), and  $[O/H]$ (ours, LTE) are denoted by green crosses, blue filled circles, and red open circles, respectively. (b)  $T_{\text{eff}}$  (theirs) vs.  $T_{\text{eff}}$  (ours). (c)  $\log g$  (theirs) vs.  $\log g$  (ours). (d)  $\nu_t$  (theirs) vs.  $\nu_t$  (ours). (e) Differences of  $\chi_{\text{low}}\theta_{\text{eff}}$  (theirs)  $-\chi_{\text{low}}\theta_{\text{eff}}$  (ours) (which define the shift in the abscissa of curve of growth) plotted against  $T_{\text{eff}}$  (ours), where  $\chi_{\text{low}} = 9.146$  eV (lower excitation potential of the O I 7771–5 triplet), and  $\theta_{\text{eff}} \equiv 5040/T_{\text{eff}}$  ( $T_{\text{eff}}$  in K). (f)  $W$  (theirs) vs.  $W$  (ours) diagram, where blue open circles, green filled circles, and red crosses correspond to O I 7771.944, 7774.166, and 7775.388 lines, respectively.

2. Since the range of  $\log g$  is rather narrow in G–K dwarfs (unlike the case of  $T_{\text{eff}}$ ), our spectroscopic  $\log g$  does not appear to be well correlated with the values based on the theoretical Hertzsprung–Russell diagram. However, the differences themselves are not so large, and are mostly

within  $\lesssim 0.1$ – $0.2$  dex. We see on average that  $\log g$  (Wang et al.) (Figure 8(b)) tends to be somewhat lower, while  $\log g$  (Ramírez et al.) (Figure 9(b)) and  $\log g$  (Luck) (Figure 10(b)) somewhat higher, as compared with our  $\log g$  derived from Fe I and Fe II lines.

3. Regarding  $\nu_t$ , while the Ramírez et al. results are almost consistent with our determination (Figure 9(c)), those of Luck show some systematic trend (Figure 10(c)), i.e., they tend to be larger for higher  $\nu_t$  (while somewhat smaller for lower  $\nu_t$ ). We can see from Figure 8(c) that  $\nu_t = 1 \text{ km s}^{-1}$  assumed by Wang et al. was not such a bad choice.
4. As to [Fe/H], good agreement is confirmed with all these studies (see Figures 8(d), 9(d), and 10(d)).

As another check for the spectroscopic  $T_{\text{eff}}$  adopted in this study, we also computed the photometric  $T_{\text{eff}}$  from  $B - V$  and [Fe/H] using the Casagrande et al. (2010) calibration based on the infrared flux method.<sup>12</sup> Comparisons between  $T_{\text{eff}}$  (this study) and  $T_{\text{eff}}$  (Casagrande et al.) are shown in Figures 11(a) and (b), where we can recognize that both are in satisfactory agreement.

It is also worthwhile to examine how our adopted spectroscopic  $\log g_{\text{spec}}$  compares with the direct value ( $\log g_{\text{TLM}}$ ) derived from  $T_{\text{eff}}$ ,  $L$  (bolometric luminosity), and  $M$  (mass). The  $L$  values were derived from  $V$  (apparent magnitude; see Table 1), *Gaia* DR2 parallax (taken from the SIMBAD database; see also Section 3.2), and the bolometric correction evaluated by interpolating Alonso et al.’s (1995) Table 4. Then,  $M$  for each star was evaluated from its position on the  $\log L$  versus  $\log T_{\text{eff}}$  diagram (see Figure 11(c)) by comparing the theoretical PARSEC tracks (Bressan et al. 2012, 2013), where fine grids are available with a step of  $0.005 M_{\odot}$  over a wide metallicity range from  $z = 0.0001$  to  $z = 0.06$  (we regard  $z = z_{\odot} \times 10^{[\text{Fe}/\text{H}]}$  as the stellar metallicity where  $z_{\odot} = 0.014$ ). The difference between  $\log g_{\text{spec}}$  and the resulting  $\log g_{\text{TLM}}$  is plotted against  $T_{\text{eff}}$  in Figure 11(d), which suggests that both are mostly consistent within  $\sim \pm 0.1$  dex (though several  $\log g_{\text{spec}}$  values are appreciably underestimated at  $T_{\text{eff}} \lesssim 5000 \text{ K}$ ; see also Figure 2(a)). These  $\log L$ ,  $M$ , and  $\log g_{\text{TLM}}$  values determined for each star are given in “tableE1.dat” of the supplementary .tar.gz package.

## 5.2. Oxygen Abundance from O I 7771–5

We go on to address the second subject of this study: whether or not credible oxygen abundances of K dwarfs can be derived from the high-excitation O I triplet lines at 7771–5 Å, for which unreasonably high abundances were reported by the Schuler et al. group in their studies on open clusters (see Section 1). As was the case for stellar parameters, Hyades G–K dwarfs can serve as an important touchstone in this respect, because they should retain almost the same (primordial) oxygen abundances in their photospheres.

Schuler et al. (2006b) derived a markedly increasing [O/H] (LTE) for Hyades dwarfs with a decrease in  $T_{\text{eff}}$ ; i.e.,  $\sim +0.2$  (at  $T_{\text{eff}} \sim 6000\text{--}5500 \text{ K}$ ),  $\sim +0.5$  (at  $T_{\text{eff}} \sim 5000 \text{ K}$ ), and  $\sim +1.0$  (at  $T_{\text{eff}} \sim 4500 \text{ K}$ ) as shown in their Figure 3. Their values are reproduced in Figure 12(a) (crosses) for 37 stars in common

with our sample. However, our results for Hyades stars turned out markedly different from theirs as manifestly seen from Figure 12(a), where [O/H](NLTE) and [O/H](LTE) (represented by filled and open symbols, respectively) are plotted against  $T_{\text{eff}}$ .<sup>13</sup> That is, our [O/H] values do not show any such progressive increase toward lower  $T_{\text{eff}}$  as reported by Schuler et al. (2006b) but are distributed around  $\sim +0.2$ , being consistent with the expectation that these stars should show similar oxygen abundances.

We investigated the cause of this discrepancy by comparing the adopted stellar parameters in both studies. Comparisons of  $T_{\text{eff}}$ ,  $\log g$ , and  $\nu_t$  are illustrated in Figures 12(b), (c), and (d), respectively. It is apparent from Figure 12(b) that a considerable disagreement exists between the Schuler et al.  $T_{\text{eff}}$  (photometric determination using colors) and our  $T_{\text{eff}}$  (spectroscopic determination from Fe lines) in the sense that the former is systematically lower by several hundred kelvin and the difference progressively increases toward lower  $T_{\text{eff}}$ . Meanwhile, a more or less reasonable consistency (excepting an outlier) is observed for  $\log g$  (Figure 12(c)), which they derived from theoretical evolutionary tracks. As to  $\nu_t$ , the Schuler et al. values tend to be somewhat higher than ours especially in the regime of larger  $\nu_t$  or higher  $T_{\text{eff}}$  (Figure 12(d)). This disagreement may be explained by the fact that they used the Allende Prieto et al. (2004) empirical formula derived for field stars and that our  $\nu_t$  values derived for Hyades dwarfs tend to be lower than those of field dwarfs at  $T_{\text{eff}} \gtrsim 5500 \text{ K}$  as remarked in Section 3.2 (see Figure 2(b)).

In view of these results along with the parameter dependence of the abundances discussed in Section 4.2, it must be the difference in  $T_{\text{eff}}$  that is mainly responsible for the considerable discrepancy in [O/H] between Schuler et al. (2006b) and this study, because the oxygen abundance from the high-excitation O I 7771–5 triplet is highly sensitive to a change in  $T_{\text{eff}}$  (Figure 6(e)) while the roles played by  $\log g$  and  $\nu_t$  are insignificant (Figures 6(f) and (g)). This can be confirmed from Figure 12(e), where  $\chi_{\text{low}}\theta_{\text{eff}} - \chi_{\text{low}}\theta_{\text{eff}}$  (Schuler et al.)  $-\chi_{\text{low}}\theta_{\text{eff}}$  (this study) ( $\theta_{\text{eff}} \equiv 5040/T_{\text{eff}}$ ; this is the expected abundance variation for neutral oxygen of dominant population due to the difference in  $T_{\text{eff}}$ ) is plotted against  $T_{\text{eff}}$  for each star. We can see from this figure that the abundance change systematically grows with a decrease in  $T_{\text{eff}}$  (from  $\sim 0.1\text{--}0.2$  dex at  $T_{\text{eff}} \sim 6000 \text{ K}$  up to  $\sim 0.6$  dex at  $T_{\text{eff}} \sim 4500 \text{ K}$ ), which reasonably explains why the Schuler et al. [O/H] values tend to be progressively larger than ours toward lower  $T_{\text{eff}}$ . Besides, we found that the equivalent widths of the O I triplet lines measured by them and used for their analysis tend to be somewhat overestimated (by several tens of percent) for weak lines ( $W_{\lambda} \lesssim 20 \text{ mÅ}$ ) in comparison with our values (Figure 12(f)), though both are consistent for lines of medium strength. This would have further enhanced the overestimation of their [O/H] in the case of such small  $W_{\lambda}$  (i.e.,  $T_{\text{eff}} \lesssim 5000 \text{ K}$ ). As such, we consider that the Schuler et al. (2006b) anomalous [O/H] results derived for Hyades dwarfs (conspicuously increasing toward lower  $T_{\text{eff}}$ ) are mainly due to their inadequate  $T_{\text{eff}}$  scale (i.e., too low by several hundred kelvin) and thus should not be taken seriously.

<sup>12</sup> While their  $T_{\text{eff}}(B - V)_0\text{--}[\text{Fe}/\text{H}]$  relation was applied to our sample of 47 Hyades and 101 field stars, we also checked how the results are changed by using other color indices. Adopting Pinsonneault et al. (2004)  $V - K_s$  and  $J - K_s$  values for Hyades dwarfs (for which 37 stars at  $4500 \text{ K} \lesssim T_{\text{eff}} \lesssim 6300 \text{ K}$  are in common with our sample), we determined  $T_{\text{eff}}^{V-K_s}$  and  $T_{\text{eff}}^{J-K_s}$  and compared them with  $T_{\text{eff}}^{B-V}$ . The mean differences were found to be  $\langle T_{\text{eff}}^{V-K_s} - T_{\text{eff}}^{B-V} \rangle = -6(\pm 46) \text{ K}$  and  $\langle T_{\text{eff}}^{J-K_s} - T_{\text{eff}}^{B-V} \rangle = +90(\pm 94) \text{ K}$ . This suggests that, while the Casagrande et al. (2010) calibration formula results in quite consistent  $T_{\text{eff}}^{V-K_s}$  and  $T_{\text{eff}}^{B-V}$ , it yields systematically higher  $T_{\text{eff}}^{J-K_s}$  than  $T_{\text{eff}}^{B-V}$  by  $\sim 100 \text{ K}$  (with somewhat larger scatter).

<sup>13</sup> The difference between [O/H](NLTE) and [O/H](LTE) (which is  $\lesssim 0.1$  dex and quantitatively insignificant) changes sign around  $T_{\text{eff}} \sim 5800 \text{ K}$ , because non-LTE corrections both for the Sun and the star are involved in [O/H] ( $\equiv A_{\text{star}}(\text{O}) - A_{\odot}(\text{O})$ ).

The results of this study suggest that consistent oxygen abundances for Hyades G–K dwarfs (i.e., without showing any systematic trend in terms of  $T_{\text{eff}}$ ) can be derived even based on the high-excitation O I 7771–5 triplet lines. The mean non-LTE  $\langle[\text{O}/\text{H}]\rangle$  for 37 stars (common to Schuler et al.) depicted in Figure 12(a) is  $+0.12$  ( $\sigma = 0.09$ ), and that for all our 47 Hyades stars (see Figure 6(c)) is identically  $+0.12$  ( $\sigma = 0.09$ ), which are favorably compared (i.e., within error bars) with  $\langle[\text{O}/\text{H}]\rangle = +0.22(\pm 0.14)$  obtained by Takeda et al. (2013) for Hyades F–G stars based on O I 6156–8 lines.

Even so, it should be kept in mind that precision of abundance determination would naturally deteriorate for K dwarfs ( $T_{\text{eff}} \lesssim 5000$  K) because the strengths of these high-excitation O I triplet lines are considerably weakened, which makes measurement more difficult (e.g., due to increased importance of blending by other lines). This can be manifestly seen from the appreciable scatter of  $[\text{O}/\text{H}]$  at  $T_{\text{eff}} \lesssim 5000$  K in Figure 12(a). Yet, we would like to stress that such a significant “ $T_{\text{eff}}$ -dependent systematic trend” as reported by Schuler et al. (2006b) is unlikely.

Admittedly, what has been argued above is specific to Hyades dwarfs and we cannot say much about the  $T_{\text{eff}}$ -dependent anomaly in  $[\text{O}/\text{H}]$  derived from O I 7771–5 (i.e., progressively increasing toward lower  $T_{\text{eff}}$ ) also reported for other cluster stars: e.g., UMa moving group (King & Schuler 2005); Pleiades and M34 (Schuler et al. 2004); NGC 752 (Maderak et al. 2013). We consider, however, that almost the same argument may also apply to the consequences of these studies, because we confirmed that the  $T_{\text{eff}}$  scale they adopted tends to be systematically lower as compared with that of Casagrande et al. (2010) (which is consistent with our spectroscopic  $T_{\text{eff}}$ ; see Figures 11(a) and (b)). The details of this examination are separately described in Appendix A (see also Table 2 and Figure 14).

Turning our attention to field stars, we compare our oxygen abundances with those derived by three previous studies (as done in Section 5.1 for stellar parameters). Panels (e) and (f) of Figures 8–10 show comparison of our (non-LTE)  $[\text{O}/\text{H}]$  and  $[\text{O}/\text{Fe}]$  values with those of Wang et al. (2009) from O I 7771–5 with non-LTE, Ramírez et al. (2013) from O I 7771–5 with non-LTE, and Luck (2017) from [O I] 6300 with LTE, respectively. These figures suggest that a rough (though not necessarily good) correlation is observed between our and their results. In addition, Figure 13 compares the non-LTE  $[\text{O}/\text{Fe}]$  versus  $[\text{Fe}/\text{H}]$  relation derived in this study for 148 G–K dwarfs (47 Hyades stars at  $6300 \text{ K} \gtrsim T_{\text{eff}} \gtrsim 4500 \text{ K}$  and 101 field stars at  $5500 \text{ K} \gtrsim T_{\text{eff}} \gtrsim 4500 \text{ K}$ ) with a similar relation obtained by Takeda & Honda (2005) based on the same O I 7771–5 triplet (with non-LTE) for early F–early K dwarfs/subgiants (at  $7000 \text{ K} \gtrsim T_{\text{eff}} \gtrsim 5000 \text{ K}$ ). It can be confirmed by comparing panels (a) and (b) of Figure 13 that quite a similar trend of  $[\text{O}/\text{Fe}]$  (i.e., increasing with a decrease in  $[\text{Fe}/\text{H}]$  with almost the same gradient) is observed for both cases. This is a reasonable consequence, because most of the sample stars belong to the thin-disk population in this study (see Section 3.2) as well as in Takeda & Honda (2005) (see Section 2.2 in Takeda 2007). For comparison, similar relations between  $[\text{O}/\text{Fe}]$  and  $[\text{Fe}/\text{H}]$  derived by Hawkins et al. (2016) for a large number of disk stars (APOGEE+*Kepler* sample) are overplotted in these figures. Although the global tendency of decreasing  $[\text{O}/\text{Fe}]$  with an increase in  $[\text{Fe}/\text{H}]$  is similar, their  $[\text{O}/\text{Fe}]$  tends to be stagnant and supersolar (i.e.,  $\gtrsim 0$ ) at

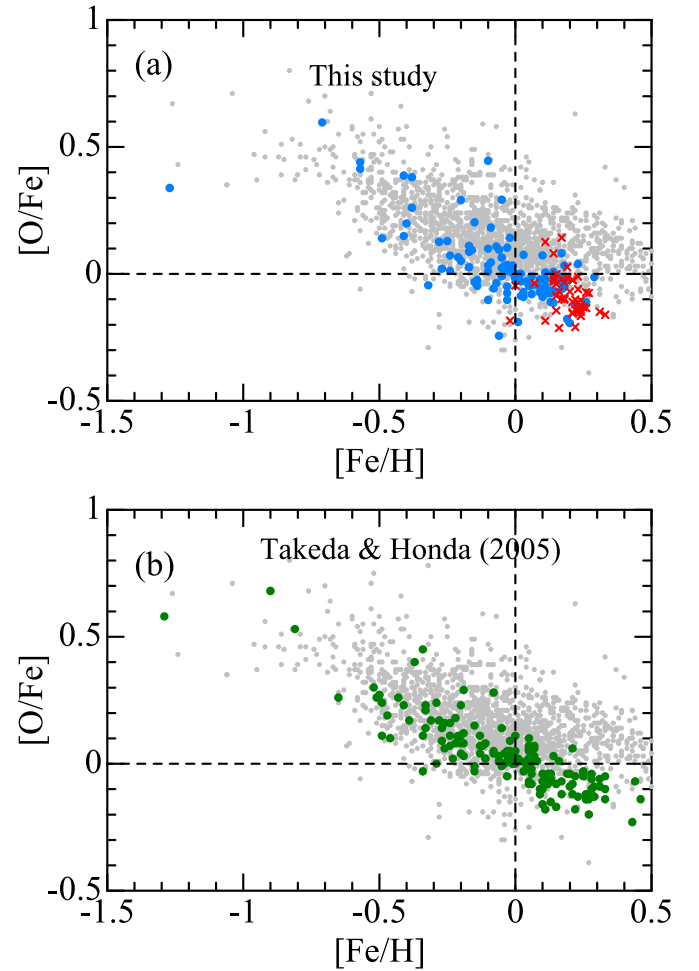


**Figure 13.** (a)  $[\text{O}/\text{Fe}]$  ratios derived in this study for each of the program stars (47 Hyades stars and 101 field stars) plotted against  $[\text{Fe}/\text{H}]$ , where the meanings of the symbols are the same as in Figure 1. (b) Takeda & Honda (2005)  $[\text{O}/\text{Fe}]$  vs.  $[\text{Fe}/\text{H}]$  relation derived for the 160 mid-F through early-K stars based on the O I 7771–5 lines. In both panels (a) and (b) similar correlations taken from Hawkins et al. (2016) are also plotted as gray dots for comparison, which were derived from high-resolution infrared spectra for a large APOGEE+*Kepler* stellar sample (APOKASC).

$[\text{Fe}/\text{H}] \gtrsim 0$  unlike our results ( $[\text{O}/\text{Fe}] \lesssim 0$  at  $[\text{Fe}/\text{H}] \gtrsim 0$ ). See also Section 4.1 in Hawkins et al. (2016).

Combining all the results mentioned above, we may conclude that oxygen abundances can be reliably determined based on the O I triplet lines at 7771–5 Å for K dwarfs (just like F and G stars), as far as stars at  $T_{\text{eff}} \gtrsim 4500$  K are concerned (actually,  $\sim 4500$  K corresponding to a spectral type of  $\sim$  K 5 is the practical lower limit of  $T_{\text{eff}}$ , below which these high-excitation O I lines become too weak to be usable).

## 6. Summary and Conclusion

It has been reported that Fe abundances of K dwarfs derived from Fe I and Fe II lines tend to show a considerable discrepancy (i.e., the latter is larger than the former), becoming progressively more serious with a decrease in  $T_{\text{eff}}$ . If this is real, the widely used spectroscopic method for determining the parameters of solar-type stars based on Fe lines (which makes use of ionization equilibrium of Fe I/Fe II) would hardly be applicable to K dwarfs, since classical model atmospheres would be no longer valid for them.

According to the recent investigations of Aleo et al. (2017) and Tsantaki et al. (2019), however, the alleged large Fe II–Fe I disagreement in K dwarfs is likely to be due to the use of blending-affected Fe II lines, and can be appreciably mitigated down to a practically insignificant level when these are removed. This suggests the necessity of re-examining another similar problem related to K dwarfs (argued, e.g., by Schuler et al. in their studies on open cluster stars) that oxygen abundances derived from the high-excitation O I 7771–5 triplet lines are strikingly overestimated (even by up to  $\sim 1$  dex), their extent becoming more prominent toward lower  $T_{\text{eff}}$ .

Motivated by this situation, we decided to re-examine whether these “spectroscopic K dwarf problems” really exist, based on spectral data of 148 G–K dwarfs (47 Hyades stars and 101 field stars). This may be checked by applying the conventional method of analysis (for determining stellar parameters and oxygen abundances) to these program stars. That is, some kind of unreasonable or inconsistent result must be observed if the classical modeling really breaks down for K dwarfs.

We determined  $T_{\text{eff}}$ ,  $\log g$ ,  $v_t$ , and [Fe/H] for all the program stars based on the equivalent widths of Fe I and Fe II lines as done by Takeda et al. (2005). Comparing our spectroscopic  $T_{\text{eff}}$  and  $\log g$  of Hyades stars with those of de Bruijne et al. (2001) (which are considered to be well established), we found that the differences are practically not so significant (in particular, no evidence was found that K dwarfs suffer larger errors than G dwarfs). This result may support Aleo et al.’s (2017) conclusion that the differences between Fe I and Fe II abundances in K dwarfs are actually not so important ( $\lesssim 0.1$  dex) at least for stars at  $T_{\text{eff}} \gtrsim 4500$  K.

The oxygen abundances of these G–K dwarfs were derived by applying the spectrum-fitting technique to the 7770–7782 Å region comprising O I 7771–5 and Fe I 7780 lines, where the non-LTE effect was taking into account for the O I lines. Regarding the [O/H] values of Hyades stars, our results turned out to be distributed around  $\sim +0.2$  (consistent with the expectation that cluster stars should have similar abundances), in marked contrast with the progressively increasing tendency (even up to  $\sim +1$ ) toward the lower  $T_{\text{eff}}$  reported by Schuler et al. (2006b).

We investigated the reason for this distinct discrepancy, and found that the lower  $T_{\text{eff}}$  scale adopted by them is the main cause, and has a large impact on the abundances derived from O I lines of high excitation. It was also confirmed that the

[O/Fe] versus [Fe/H] relation we obtained for 101 field mid G–mid K stars is quite similar to that derived by Takeda & Honda (2005) for 160 stars (mainly F–G type), which means that K dwarfs cannot be exceptionally anomalous in terms of oxygen abundance determination based on the O I 7771–5 triplet.

In summary, we conclude for K dwarfs that their atmospheric parameters can be spectroscopically evaluated to a sufficient precision in the conventional manner using Fe lines (because the classical Saha–Boltzmann equation for Fe I/Fe II is still not a bad assumption) and oxygen abundances can be reliably established from the high-excitation O I 7771–5 triplet (just like F–G dwarfs), so far as stars of  $T_{\text{eff}} \gtrsim 4500$  K are concerned.

This investigation is based in part on the data collected at Subaru Telescope, which is operated by the National Astronomical Observatory of Japan. Data reduction was in part carried out by using the common-use data analysis computer system at the Astronomy Data Center (ADC) of the National Astronomical Observatory of Japan. This research has made use of the SIMBAD database, operated by CDS, Strasbourg, France. This work also used the data from the European Space Agency (ESA) mission *Gaia*, processed by the *Gaia* Data Processing and Analysis Consortium (DPAC). Funding for the DPAC has been provided by national institutions, in particular the institutions participating in the *Gaia* Multilateral Agreement.

## Appendix A

### Impact of Effective Temperature Scale on [O/H] in Previous Studies of Open Clusters

We showed in Section 5.2 that the conspicuous excess of [O/H] increasing toward a lower  $T_{\text{eff}}$  concluded by Schuler et al. (2006b) for Hyades stars could be interpreted as mainly due to the systematically lower  $T_{\text{eff}}$  scale they adopted (see Figure 12). Regarding the similar tendencies in [O/H] (based on the high-excitation O I 7771–5 triplet lines) also reported by several authors for open clusters other than Hyades (i.e., UMa moving group, M34, Pleiades, NGC 752; see Section 1), we are unable to check them directly as done in Figure 12. Still, however, we can examine whether the  $T_{\text{eff}}$  scales adopted by those previous studies are reasonable and how they affect the [O/H] trends.

We first postulate that Casagrande et al.’s (2010) calibration yields reasonably correct  $T_{\text{eff}}$ , which we confirmed to be

**Table 2**  
Published [O/H] Derivations from O I 7771–5 Lines for Open Cluster Stars

Cluster (1)	Ref. (2)	Figure (3)	[O/H] <sub>5000</sub> (4)	[O/H] <sub>6000</sub> (5)	$T_{\text{eff}}$ formula (6)	[Fe/H] (7)	Remark (8)
Hyades	SCH06	Figure 3	$\sim 0.5$	$\sim 0.2$	Equation (1)	+0.15	
Pleiades	SCH04	Figure 1	$\sim 0.9$	$\sim 0.2$	Equation (2)	+0.01	See also Figure 4 in KS05.
M34	SCH04	Figure 1	$\sim 0.8$	$\sim 0.1$	...	+0.07	Spectroscopic $T_{\text{eff}}$ .
UMa group	KS05	Figure 4	$\sim 0.3$	$\sim 0.1$	Equation (3)	−0.08	
Hyades	MAD13	Figure 4	...	$\sim 0.2$	Equation (1)	+0.15	Lowest $T_{\text{eff}} \sim 5400$ K, where [O/H] $\sim 0.3$ .
NGC 752	MAD13	Figure 5	$\sim 0.7$	$\sim -0.1$	Equation (1)	−0.06	$E(B - V) = 0.035$ was adopted.

**Note.** (1) Cluster name. (2) Reference key: SCH06—Schuler et al. (2006b), SCH04—Schuler et al. (2004), KS05—King & Schuler (2005), MAD13—Maderak et al. (2013). (3) Figure number of the relevant paper where [O/H] versus  $T_{\text{eff}}$  plots for cluster stars are presented. (4) Rough value of [O/H] at  $T_{\text{eff}} \sim 5000$  K. (5) Rough value of [O/H] at  $T_{\text{eff}} \sim 6000$  K. (6)  $T_{\text{eff}}$  versus  $(B - V)_0$  formula adopted in the relevant study for evaluation of  $T_{\text{eff}}$ . (7) [Fe/H] of the cluster, which we used for evaluation of  $T_{\text{eff}}^{\text{Casagrande}}$  (see Figure 14(b)) using the Casagrande et al. (2010) relation. (8) Specific remark.

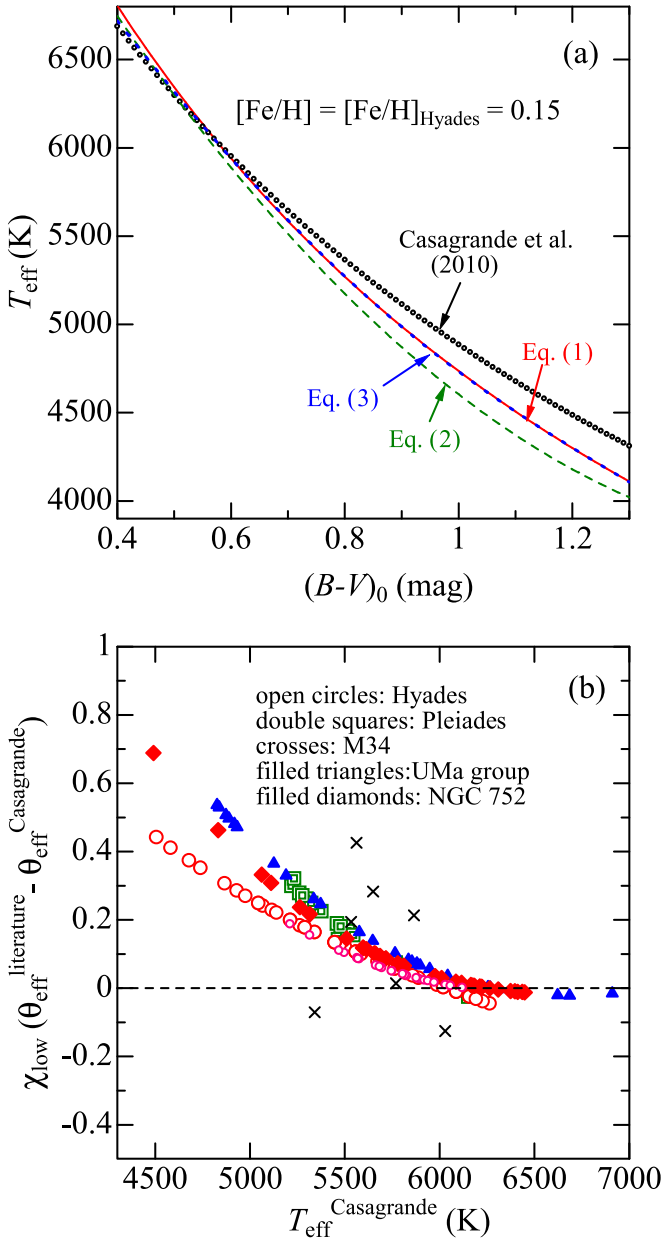


**Figure 14.** (a) Comparison of three  $T_{\text{eff}}$  vs.  $B - V$  relations (lines) used in previous studies on the  $[\text{O}/\text{H}]$  trends of open cluster stars (see Table 2) with that of Casagrande et al. (2010) (black filled circles), where  $[\text{Fe}/\text{H}]$  is set at  $+0.15$  ( $=[\text{Fe}/\text{H}]_{\text{Hyades}}$ ) for all cases. Red solid line—Equation (1), green dashed line—Equation (2), and blue dotted line—Equation (3). Differences of  $\chi_{\text{low}}\theta_{\text{eff}}$  (literature)  $-\chi_{\text{low}}\theta_{\text{eff}}$  (Casagrande et al.) (see the caption of Figure 12(e) for the meanings of  $\theta_{\text{eff}}$  and  $\chi_{\text{low}}$ ) are plotted against  $T_{\text{eff}}$  (Casagrande et al.), where  $T_{\text{eff}}$  (literature) is the actual value used by the relevant study and  $T_{\text{eff}}$  (Casagrande et al.) was calculated according to Casagrande et al. (2010) along with each star’s  $B - V$  and cluster  $[\text{Fe}/\text{H}]$ . Large open circles—Hyades (SCH06), small open circles—Hyades (MAD13), double squares—Pleiades (SCH04), crosses—M34 (SCH04), filled triangles—UMA moving group (KS05), and filled diamonds—NGC 752 (MAD13). (See the caption of Table 2 for the key to the reference code.) Note that the colors of the symbols are chosen to match those of the lines in panel (a) corresponding to the  $T_{\text{eff}}$  vs.  $B - V$  formula adopted in each paper.

consistent with our spectroscopic  $T_{\text{eff}}$  (see Figures 11(a) and (b)). Since  $T_{\text{eff}}$  values were derived photometrically from  $B - V$  colors using any of the following three formulas in most of these relevant studies (see Table 2 for a brief summary), the effect we want to examine is essentially attributed to the

difference of these equations from that of Casagrande et al. (2010):

$$T_{\text{eff}} = 5040 / (0.5247 + 0.5396(B - V)_0) + 701.7(B - V)_0([\text{Fe}/\text{H}] - [\text{Fe}/\text{H}]_{\text{Hyades}}), \quad (1)$$

$$T_{\text{eff}} = 1808(B - V)_0^2 - 6103(B - V)_0 + 8899, \quad (2)$$

and

$$T_{\text{eff}} = 8344 - 3631.32(B - V)_0 - 2211.81(B - V)_0^2 + 3365.44(B - V)_0^3 - 1033.62(B - V)_0^4 + 701.7([\text{Fe}/\text{H}] - [\text{Fe}/\text{H}]_{\text{Hyades}}), \quad (3)$$

where  $T_{\text{eff}}$  is in K,  $(B - V)_0$  is the reddening-corrected  $B - V$  color,  $[\text{Fe}/\text{H}]$  is the metallicity of a star, and  $[\text{Fe}/\text{H}]_{\text{Hyades}}$  is the Hyades metallicity (assumed to be 0.15 in this study). These  $T_{\text{eff}}$  versus  $(B - V)_0$  relations of Equations (1)–(3) are compared with that of Casagrande et al. (2010) in Figure 14(a), where we can see that all the former three tend to yield systematically lower  $T_{\text{eff}}$  than the latter at  $(B - V)_0 \gtrsim 0.6$  with discrepancies increasing toward lower  $T_{\text{eff}}$ .

For each star,  $T_{\text{eff}}^{\text{Casagrande}}$  was computed from  $(B - V)_0$  (taken from the relevant paper) and assumed cluster  $[\text{Fe}/\text{H}]$  (see Table 2) according to Casagrande et al.’s (2010) recipe and compared with the literature value ( $T_{\text{eff}}^{\text{literature}}$ ) actually adopted therein. The differences  $\chi_{\text{low}}\theta_{\text{eff}}^{\text{literature}} - \chi_{\text{low}}\theta_{\text{eff}}^{\text{Casagrande}}$  (see the caption of Figure 12(e) for the meanings of  $\theta_{\text{eff}}$  and  $\chi_{\text{low}}$ ) are plotted against  $T_{\text{eff}}^{\text{Casagrande}}$  in Figure 14(b), from which we can read the following characteristics.

1. In all cases, the differences between  $\chi_{\text{low}}\theta_{\text{eff}}^{\text{literature}}$  and  $\chi_{\text{low}}\theta_{\text{eff}}^{\text{Casagrande}}$ , which correspond to the expected overestimation of  $[\text{O}/\text{H}]$  due to an underestimated  $T_{\text{eff}}$  (see Section 5.2), tend to progressively increase with a lowering of  $T_{\text{eff}}$ ; i.e., from  $\sim 0.0$  dex (at  $\sim 6000$  K) to  $\sim 0.3$ – $0.5$  dex (at  $\sim 5000$  K). This reasonably explains the  $T_{\text{eff}}$ -dependent tendency of  $[\text{O}/\text{H}]$  concluded in their papers (see Table 2) at least qualitatively, which indicates that the inappropriate  $T_{\text{eff}}$  scale is the main cause for the trend.
2. Quantitatively, however, this  $T_{\text{eff}}$ -related correction seems to be insufficient to account for the differences ( $[\text{O}/\text{H}]_{5000} - [\text{O}/\text{H}]_{6000}$ ) ranging from  $\sim 0.2$  dex to  $\sim 0.7$  dex (Table 2), which means that some other factors (such as an underestimation of  $W_\lambda$  for the very weak line case at the low- $T_{\text{eff}}$  regime; see Figure 12(f)) may also be involved.
3. In particular, as seen from Figure 2 of Schuler et al. (2004), the  $d[\text{O}/\text{H}]/dT_{\text{eff}}$  gradient of Pleiades and M34 cluster stars at  $T_{\text{eff}} \lesssim 5200$  K appears to become abruptly steeper. Since these two open clusters are younger than the Hyades and thus stellar activity should be higher, the possibility cannot be excluded that some activity-related effect might influence the strength of the high-excitation O I triplet for these cases. Accordingly, oxygen abundances from O I 7771–5 lines for dwarfs of these younger clusters at the  $T_{\text{eff}}$  regime of  $4500 \text{ K} \lesssim T_{\text{eff}} \lesssim 5500 \text{ K}$  may be worth careful reinvestigation based on reliable  $T_{\text{eff}}$  scales.

## Appendix B Supplementary Materials

Two tables are provided in the supplementary “data.tar.gz” package. This package contains the basic data of the program stars along with their Fe and O abundances, the equivalent widths of Fe I and Fe II lines, and the line-by-line abundances corresponding to the final atmospheric parameters.

### References

- Aleo, P. D., Sobotka, A. C., & Ramírez, I. 2017, *ApJ*, **846**, 24
- Allende Prieto, C., Barklem, P. S., Lambert, D. L., & Cunha, K. 2004, *A&A*, **420**, 183
- Alonso, A., Arribas, S., & Martínez-Roger, C. 1995, *A&A*, **297**, 197
- Asplund, M. 2009, *ARA&A*, **47**, 481
- Bressan, A., Marigo, P., Girardi, L., et al. 2012, *MNRAS*, **427**, 127
- Bressan, A., Marigo, P., Girardi, L., Nanni, A., & Rubele, S. 2013, *EPJWC*, **43**, 3001
- Casagrande, L., Ramírez, I., Meléndez, J., Bessel, M., & Asplund, M. 2010, *A&A*, **512**, A54
- Cayrel, R. 1988, in Proc. IAU Symp. 132, The Impact of Very High S/N Spectroscopy on Stellar Physics, ed. G. Cayrel de Strobel & M. Spite (Dordrecht: Kluwer), 345
- de Bruijne, J. H. J., Hoogerwerf, R., & de Zeeuw, P. T. 2001, *A&A*, **367**, 111
- Dutra-Ferreira, L., Pasquini, L., Smiljanic, R., Porto de Mello, G. F., & Steffen, M. 2016, *A&A*, **585**, A75
- Gaia Collaboration et al., Prusti, T., & de Bruijne, J. H. J. 2016, *A&A*, **595**, A1
- Gaia Collaboration, Brown, A. G. A., Vallenari, A., et al. 2018, *A&A*, **616**, A1
- Grevesse, N., & Sauval, A. J. 1998, *SSRv*, **85**, 161
- Hawkins, K., Masseron, T., Jofré, P., et al. 2016, *A&A*, **594**, A43
- Ibukiyama, A., & Arimoto, N. 2002, *A&A*, **394**, 927
- King, J. R., & Schuler, S. C. 2005, *PASP*, **117**, 911
- Kotoneva, E., Flynn, C., Chiappini, C., & Matteucci, F. 2002, *MNRAS*, **336**, 879
- Kotoneva, E., Shi, J. R., Zhao, G., & Liu, Y. J. 2006, *A&A*, **454**, 833
- Kurucz, R. L. 1993, ATLAS9 Stellar Atmosphere Programs and 2 km/s Grid (Cambridge, MA: Smithsonian Astrophysical Observatory)
- Kurucz, R. L., & Bell, B. 1995, Atomic Line Data, Kurucz CD-ROM No. 23 (Cambridge, MA: Smithsonian Astrophysical Observatory)
- Kurucz, R. L., Furenlid, I., Brault, J., & Testerman, L. 1984, Solar Flux Atlas from 296 to 1300 nm (Sunspot, NM: National Solar Observatory)
- Luck, R. E. 2017, *AJ*, **153**, 21
- Maderak, R. M., Deliyannis, C. P., King, J. R., & Cummings, J. D. 2013, *AJ*, **146**, 143
- Pinsonneault, M. H., Terndrup, D. M., Hanson, R. B., & Stauffer, J. R. 2004, *ApJ*, **600**, 946
- Ramírez, I., Allende Prieto, C., & Lambert, D. L. 2013, *ApJ*, **764**, 78
- Ryabchikova, T., Piskunov, N., Kurucz, R. L., et al. 2015, *PhysS*, **90**, 054005
- Schuler, S. C., Hatzes, A. P., King, J. R., Kürster, M., & The, L.-S. 2006a, *AJ*, **131**, 1057
- Schuler, S. C., King, J. R., Hobbs, L. M., & Pinsonneault, M. H. 2004, *ApJL*, **602**, L117
- Schuler, S. C., King, J. R., Terndrup, D. M., et al. 2006b, *ApJ*, **636**, 432
- Schuler, S. C., Plunkett, A. L., King, J. R., & Pinsonneault, M. H. 2010, *PASP*, **122**, 766
- Takeda, Y. 1995, *PASJ*, **47**, 287
- Takeda, Y. 2003, *A&A*, **402**, 343
- Takeda, Y. 2007, *PASJ*, **59**, 335
- Takeda, Y. 2008, in The Metal-Rich Universe, ed. G. Israelian & G. Meynet (Cambridge: Cambridge Univ. Press), 308
- Takeda, Y., & Honda, S. 2005, *PASJ*, **57**, 65
- Takeda, Y., Honda, S., Ohnishi, T., et al. 2013, *PASJ*, **65**, 53
- Takeda, Y., Ohkubo, M., & Sadakane, K. 2002, *PASJ*, **54**, 451
- Takeda, Y., Ohkubo, M., Sato, B., Kambe, E., & Sadakane, K. 2005, *PASJ*, **57**, 27, [Erratum: *PASJ*, **57**, 415]
- Takeda, Y., Sato, B., Omiya, M., & Harakawa, H. 2015, *PASJ*, **67**, 24
- Tsantaki, M., Santos, N. C., Sousa, S. G., Delgado-Mena, E., & Adibekyan, V. 2019, *MNRAS*, **485**, 2772
- Wang, X. M., Shi, J. R., & Zhao, G. 2009, *MNRAS*, **399**, 1264
- Yong, D., Lambert, D. L., Allende Prieto, C., & Paulson, D. 2004, *ApJ*, **603**, 697